

PART I: EXPERIMENTAL SPECTROSCOPIC TEMPERATURE
MEASUREMENTS IN THE REFLECTED WAVE REGION OF A
SHOCK TUBE USING THE OH $^2\Sigma \rightarrow ^2\Pi$ BAND SYSTEM

PART II: SHOCK TUBE MEASUREMENTS OF THE
ABSORPTION OSCILLATOR STRENGTH FOR THE $^2\Sigma \rightarrow ^2\Pi$
ELECTRONIC BAND SYSTEM OF OH

Thesis by
Ronald Watson

In Partial Fulfillment of the Requirements
For the Degree of
Doctor of Philosophy

California Institute of Technology
Pasadena, California

1963

ACKNOWLEDGMENTS

The author wishes to express his appreciation to Professor S. S. Penner for his helpful advice and guidance during the course of the research presented here.

Grateful appreciation is also extended to the National Science Foundation for a Science-Faculty Fellowship covering the period from 1959 to 1961 and to the Ford Foundation for assistance from their Fellowship and Loan Program from 1961 to 1963. The United States Air Force contributed financial support to the research under Grant No. AFOSR-7163 with the California Institute of Technology.

The assistance of Mrs. Barbara Mullican and Mrs. Roberta Duffy in the preparation of this manuscript is also gratefully acknowledged.

ABSTRACT FOR PART I

Experimental measurements of the population temperature behind the reflected shock in a shock tube are presented. Emission from two wavelength intervals of the OH ${}^2\Sigma \rightarrow {}^2\Pi$ electronic band system was measured photoelectrically, the signals observed being generated by a narrow core of hot gas in the reflected shock region looking axially up the tube. The ratio of the rate of increase of intensity with unit increase of optical depth in the two spectral regions is a unique function of the temperature for a transparent gas. The linearity of the signal increase with time represents an experimental verification of the transparency and equilibration of the test gas.

In the temperature range of 3300-4300^oK ($M_s \sim 4$), the measured spectroscopic temperature was in good agreement with the calculated equilibrium temperature, the estimated accuracy of the spectroscopic temperature being $\pm 75^{\circ}$ K. A relaxation time of about 25 μ sec was observed for the (2, 2) and (3, 3) vibration bands to reach statistical equilibrium with the lower (0, 0) and (1, 1) vibrational levels in the ${}^2\Sigma$ state from which the emission occurred.

ABSTRACT FOR PART II

Previous shock tube measurements of the oscillator strength of the OH ${}^2\Sigma \rightarrow {}^2\Pi$ band system made in this Laboratory⁽¹⁾ have been corrected. Light scattering in the absolute intensity calibration has

been eliminated and a continuous flushing technique was used for preparation and introduction of the water vapor-argon test gas mixture into the tube. The experimental technique remains essentially the same as in the earlier studies: hot gas samples at 3100-3500°K were produced behind the reflected shock and the linear rate of increase of absolute spectral intensity in the transparent gas region was measured by monitoring emission from axial observations in the shock tube.

The absorption electronic f-number for the ${}^2\Sigma \rightarrow {}^2\Pi$ band system has been determined from the measurements as $(3.9 \pm 0.9) \times 10^{-3}$. This value should be compared with Carrington's⁽²⁾ result of 1.4×10^{-3} from absorption measurements in flames, and Oldenberg and Rieke's⁽³⁾ value of 1.3×10^{-3} and Dyne's⁽⁴⁾ value of 0.7×10^{-3} from measurements in absorption cells.

TABLE OF CONTENTS

<u>Section</u>	<u>Title</u>	<u>Page</u>
	ACKNOWLEDGMENTS	i
	ABSTRACTS	ii
	TABLE OF CONTENTS	iv
PART I: EXPERIMENTAL SPECTROSCOPIC TEMPERATURE MEASUREMENTS IN THE REFLECTED WAVE REGION OF A SHOCK TUBE USING THE OH ${}^2\Sigma \rightarrow {}^2\Pi$ BAND SYSTEM		
I.	INTRODUCTION	1
II.	THEORETICAL CONSIDERATIONS	6
III.	NUMERICAL CALCULATIONS FOR OH	14
IV.	EXPERIMENTAL FACILITIES	23
	A. The Shock Tube and Associated Measuring Apparatus	23
	B. The Optical System	26
	C. The Gas-Handling System	28
V.	EXPERIMENTAL PROCEDURE	33
	A. Determination of the Relative Intensity Ratio of K_{r_2} / K_{r_1}	33
	B. Thermodynamic Properties of the Gas Behind the Shock Wave	34
VI.	EXPERIMENTAL RESULTS	35
	A. Estimate of Accuracy	41
	B. Comparison with Other Experiments	42
	C. Vibrational Relaxation of OH	43
VII.	CONCLUSIONS	44
	REFERENCES FOR PART I	45

<u>Section</u>	<u>Title</u>	<u>Page</u>
	PART II: SHOCK TUBE MEASUREMENTS OF THE ABSORPTION OSCILLATOR STRENGTH FOR THE $^2\Sigma^-2\Pi$ ELECTRONIC BAND SYSTEM OF OH	
I.	INTRODUCTION	48
II.	THEORETICAL CONSIDERATIONS	53
	A. The Shock Tube Experiment	53
	B. The Absolute Intensity Calibration	62
III.	EXPERIMENTAL EQUIPMENT	66
	A. Shock Tube Exit Optics	66
	B. Calibration Optics	75
IV.	THERMODYNAMIC PROPERTIES OF THE GAS BEHIND THE SHOCK WAVE	77
V.	DISCUSSION OF RESULTS	81
	REFERENCES FOR PART II	85

PART I - EXPERIMENTAL SPECTROSCOPIC TEMPERATURE
MEASUREMENTS IN THE REFLECTED WAVE REGION
OF A SHOCK TUBE USING THE OH $^2\Sigma \rightarrow ^2\Pi$ BAND
SYSTEM

I. INTRODUCTION

The shock tube has been used extensively for a number of years in chemical kinetic measurements, absolute emission studies, and other spectroscopic experiments (see for example Refs. 1-5). The popularity of the shock tube is due to the fact that the shock adds energy to the test gas and raises its temperature uniformly and almost instantaneously to a thermodynamic state that is readily determined from the conservation relations of fluid mechanics. Many observers have utilized the region behind the reflected shock wave to obtain relatively high gas temperatures, without being forced to use heated hydrogen drivers or excessively high driver pressures.

In recent years, however, much discussion of the conditions behind reflected shocks has occurred in the literature. ⁽⁶⁻¹⁰⁾ Varying agreement may be noted in these studies on the deviation from ideal behavior caused primarily by the interaction of the reflected shock wave with the boundary layer set up by the incident shock wave.

Relatively small temperature uncertainties may be particularly troublesome in some absolute emission measurements.

The oscillator strength or f-number, ⁽¹¹⁾ depends on the relation of gas emission to black body emission. In the ultraviolet region, the blackbody function as well as the species composition, varies rapidly with temperature. Thus, a temperature uncertainty of a few hundred degrees may lead to a large uncertainty in the f-number.

An example of an experiment faced with this difficulty is the measurement of the electronic f-number of the OH $^2\Sigma \rightarrow ^2\Pi$ band system which has been performed in this Laboratory using spectroscopic measurements of emission behind the reflected shock. ⁽⁴⁾ The band head for this system lies at 3064A. At $\sim 3500^\circ\text{K}$, an uncertainty of about 200°K leads to an uncertainty of a factor of 3 in the f-number.

Because of this sensitive dependence of f-number on temperature, and because of the questions associated with observations in the reflected shock region, it was felt that a direct measurement of the temperature of the OH species would be highly desirable. Since the testing time in shock tubes is relatively short, and since a measuring device must not perturb the high-speed flow, optical procedures appeared to be the most attractive way to measure the temperature.

Many spectroscopic techniques for measuring equilibrium temperatures are known and have been discussed in the literature (see for example, Ref. 12). Two of the most widely known procedures,

namely, the line-reversal method and the rotational line intensity method, have been employed in recent years to obtain gas temperatures in shock tubes.^(13,14) Both of these methods depend on emission from substances added to the gas, the assumption being that the additive is in thermal equilibrium with the other gases, thus furnishing a measure of the gas "temperature".

Gaydon and his co-workers introduced sodium chloride into the test gas and observed the emission or absorption of sodium lines relative to light emission from a lamp ($T \approx 2500^{\circ}\text{K}$).⁽¹³⁾ This line-reversal technique is relatively free from systematic errors but has the limitation of requiring a source of known temperature and emissivity and is, therefore, practically limited to measuring gas temperatures below about 4000°K , although pulsed or other special types of light sources may extend the usable temperature range.^(15,32)

The rotational line intensity method was used by Parkinson and Nicholls on the CN molecule.⁽¹⁴⁾ These authors measured the relative intensities of rotational lines in CN bands of spectrograms obtained in emission from compounds containing carbon and nitrogen, the compounds being painted on a Mylar membrane clamped in the tube. Use of the rotational line technique requires high spectral resolution and a very fast (low f/D) optical system, as well as careful calibration of the film. In many cases, the available intensity and/or resolution may not be sufficient to permit application of this method

in shock tubes. A wider spectrograph entrance slit increases the light flux into the instrument but reduces the spectral resolution.

Another technique used to measure shock tube gas temperatures involves the absorption of light by O_2 bands in the 2280-2870A range and has been used by Wurster and Treanor.⁽¹⁶⁾ Light from a xenon-filled flash lamp was passed through the shock tube and specific regions of the absorption spectrum were recorded photoelectrically. The calculated temperature dependence of the absorption thus allows the temperature to be defined. This broad-band absorption method has the advantage of being a direct measurement on the gas species of interest, but it requires knowledge of spectral line shapes and a high-intensity light source in the desired spectral region.

An alternative technique, which forms the basis for the present study and which was described previously,⁽¹²⁾ involves measurement of the light emission from many rotational lines simultaneously. For a transparent gas at equilibrium,* the integrated emission (or absorption) for a vibration-rotation band is given, in terms of the vibrational absorption oscillator strength $f_{nn'}$, as

$$\alpha_{\text{band}} = \frac{\pi e^2}{m_e c} \frac{N_l}{p} f_{nn'} \{1 - \exp(-hc\bar{\omega}_{0,0}/kT)\} \quad (1)$$

* Throughout the discussion, an equilibrium population distribution in an isothermal system is assumed.

where $e^2/m_e c^2$ is the classical electron radius, N_l the concentration of emitting molecules in the lower vibrational state n' , p the partial pressure of the emitting molecule, and $\bar{\omega}_{0,0}$ the wavenumber at the band head. For a set of given initial conditions in a shock tube, the quantity α_{band} is completely determined by the temperature and thus the light flux emitted by a molecular band is also completely determined.

There is a disadvantage, however, in attempting to utilize Eq. 1 in a shock-tube experiment, even if the f-number is known precisely, since an absolute calibration of the response of the optical system is required. Although absolute calibrations have been performed in f-number experiments in shock tube studies, ^(4, 5, 17) the calibration is difficult and agreement between f-number measurements is rarely better than within a factor of two. ^(17, 18, 19) In fact, a shock tube temperature measurement based on the existing atomic f-numbers gave incorrect temperatures apparently because the f-number data used were in error. ^(20, 5)

A simpler shock tube experiment may be performed by monitoring simultaneously the emission from two or more wavelength regions of a vibration-rotation band with monochromators (or their equivalent filters) having relatively wide entrance slits and using photomultiplier detectors to obtain signals whose ratio is a unique function of the emitting gas temperature. These relative intensity measurements in emission have the advantage of not requiring an

absolute intensity calibration or the use of an external light source. Furthermore, the optical arrangement required for the temperature measurements is essentially the same as that used for f-number experiments, thus furnishing a direct temperature measurement on the species while absolute emission observations are being made.

The procedure for the calculations involved in obtaining the functional relationship defining temperature in terms of intensity ratios will now be outlined. These methods are, of course, applicable to any molecule if the proper data are available. Detailed calculations and experimental results are, however, presented only for the OH molecule.

II. THEORETICAL CONSIDERATIONS^{*}

The method used in this section is to consider first the contribution from a single line to the light flux incident on a detector in the exit plane of a monochromator and then to sum over all of the lines passed by the monochromator to obtain the total flux, and hence the voltage produced, by the detector system.

For an isolated spectral line centered at the wavenumber ω_0 , the steradiancy emitted by the hot gas at the shock tube end wall is the integral of the product of the emissivity times the black-body function over the entire spectrum, i. e.,

* The discussion presented here and in some of the following sections is essentially the same as that given by the author in Technical Report No. 39, Nonr-220(45), NR 015 401, California Institute of Technology, June, 1962.

$$B_{\text{line}} = \int_0^{\infty} \epsilon_{\omega} B_{\omega}^{\circ} d\omega \quad (2)$$

where ϵ_{ω} is the spectral emissivity of the emitting gas and B_{ω}° the blackbody spectral steradiancy.

The monochromator serves as a filter and has a non-uniform response to incident light of different wavelengths, the usual slit function response form being triangular in shape (see, for example, Ref. 21, Chap. 5). As a result, the intensity at each point in the spectral band-pass, $2\Delta\omega^*$, is weighted by the relative height of the slit function and Eq. 2 should be replaced by the expression

$$B_L = \int_{\omega_0 - \Delta\omega^*}^{\omega_0 + \Delta\omega^*} \epsilon_{\omega} B_{\omega}^{\circ} g_{\omega} d\omega \quad (3)$$

where B_L is the steradiancy of the line at the exit plane of the monochromator and g_{ω} is the monochromator slit response function. The range $2\Delta\omega^*$ in the integration is the wavenumber interval in which the slit function g_{ω} is non-zero. The transmission losses in the shock tube windows and in the monochromator have been disregarded since they are essentially constant over the total wavenumber range ($\sim 150\text{\AA}$) used in this study.

In terms of the spectral absorption coefficient (P_{ω}) and the optical depth (X), which is the product of the partial pressure (p) of the emitting species and of the geometrical path length (L), Eq. 3 becomes

$$B_L = \int_{\omega_0 - \Delta\omega^*}^{\omega_0 + \Delta\omega^*} [1 - \exp(-P_\omega X)] B_\omega^0 g_\omega d\omega .$$

For an optically thin gas, $P_\omega X \ll 1$ and, thus,

$$B_L = X \int_{\omega_0 - \Delta\omega^*}^{\omega_0 + \Delta\omega^*} P_\omega B_\omega^0 g_\omega d\omega . \quad (4)$$

The widths of individual spectral lines are so small that B_ω^0 and g_ω are effectively constant over the region where P_ω is non-zero.

Equation 4 may therefore be written as

$$B_L = B_{\omega_0}^0 g_{\omega_0} X \int_{\omega_0 - \Delta\omega^*}^{\omega_0 + \Delta\omega^*} P_\omega d\omega \equiv B_{\omega_0}^0 g_{\omega_0} X S_{\omega_0}$$

or, for the i th spectral line centered at ω_i within the slit function base $2\Delta\omega^*$,

$$B_{L_i} = B_{\omega_i}^0 g_{\omega_i} X S_{\omega_i} \quad (5)$$

where S_{ω_i} is the integrated intensity of the i th spectral line.

The integrated intensity is, in principle, calculable and may be expressed in terms of the square of the matrix element for the dipole moment of the i th line (see, for example, Ref. 21, Chap. 7), i.e.,

$$S_{\omega_i} = \frac{8\pi^3}{3hc} \omega_i \frac{N_{\ell_i}}{\rho} \frac{1}{g_{\ell_i}} [1 - \exp(-hc\omega_i/kT)] |R_{\ell u}|_i^2$$

where N_{ℓ_i} is the number of emitting molecules per unit volume in the

lower state ℓ for the line considered, $g_{\ell i}$ represents the degeneracy of the lower state, and $|R_{\ell u}|_i^2$ is the square of the matrix element for the i th line (for a transition from the upper state u to the lower state ℓ).

To a high degree of approximation, the wave functions describing the behavior of the electronic, vibrational, and rotational states of a diatomic molecule are separable⁽²²⁾ and the square of the total matrix element $|R_{\ell u}|_i^2$ may be written as

$$|R_{\ell u}|_i^2 = |R_{e\ell}(\bar{r}_e)|^2 |p_{nn'}|^2 |p_{kk'}|_i^2$$

where $|R_{e\ell}(\bar{r}_e)|^2$ is the square of the electronic matrix element, $|p_{nn'}|^2$ represents the square of the vibrational matrix element, and $|p_{kk'}|_i^2$ is the square of the rotational matrix element for the i th line.

The electronic term, $|R_{e\ell}|^2$, is not known in absolute magnitude since it represents essentially the uncertain electronic oscillator strength for the band system; it is, however, assumed to be constant for the system. The vibrational term is the overlap integral and is taken to be a constant for a particular vibration-rotation band; it is calculable if one chooses the proper potential functions to describe the oscillator behavior of the molecule.⁽²³⁾ The $|p_{kk'}|_i^2$ terms are the rotational transition probabilities for the i th line and are known for OH, within a constant factor, from the high-resolution spectrographic work of Dieke and Crosswhite.⁽²⁴⁾

The steradiancy for the i th line now becomes

$$B_{L_i} = \frac{8\pi^3}{3hc} \omega_i \frac{N_{\ell_i}}{p} \frac{X}{g_{\ell_i}} [1 - \exp(-hc\omega_i/kT)] |R_{e\ell}|^2 |P_{nn'}|^2 |P_{kk'}|^2 B_{\omega_i}^0 g_{\omega_i}. \quad (6)$$

Since the black-body spectral steradiancy is

$$B_{\omega_i}^0 = 2hc^2 \omega_i^3 \frac{1}{[\exp(hc\omega_i/kT) - 1]},$$

Eq. 6 takes the form

$$B_{L_i} = \frac{16\pi^3 c \omega_i^4}{3p} \frac{N_{\ell_i}}{g_{\ell_i}} X [\exp(-hc\omega_i/kT)] |R_{e\ell}|^2 |P_{nn'}|^2 |P_{kk'}|^2 g_{\omega_i}. \quad (7)$$

For statistical equilibrium,

$$N_{\ell_i} = \frac{N_T}{Q} g_{\ell_i} \exp(-E_{\ell_i}/kT)$$

where N_T is the total concentration of the emitting species in all energy states, Q is the internal partition function, and $E_{\ell_i} = E_{u_i} - hc\omega_i$. Thus, Eq. 7 becomes

$$B_{L_i} = \frac{16\pi^3 c X}{3p} \frac{N_T}{Q} [\exp(-E_{u_i}/kT)] \omega_i^4 |R_{e\ell}|^2 |P_{nn'}|^2 |P_{kk'}|^2 g_{\omega_i}. \quad (8)$$

Assuming ideal gas behavior,

$$\frac{N_T}{p} = \frac{1}{kT}$$

and Eq. 8 may be written as

$$\frac{B_{L_i}}{X} = \frac{16\pi^3 c}{3kT} \frac{\exp(-E_{u_i}/kT)}{Q} \omega_i^4 |R_{e\ell}|^2 |P_{nn'}|^2 |P_{kk'}|^2 g_{\omega_i} \quad (9)$$

which is the steradiancy emitted per unit optical depth from the i th line of a transparent gas.

Since a monochromator passes radiation from many spectral lines within the slit function base, Eq. 9 must be summed over all of the lines in all the branches of all bands of the band system considered that lie within the slit function base. Thus the total steradiancy incident on the detector at the exit slit, per unit optical depth X , becomes

$$\frac{B}{X} = \frac{1}{X} \left[\sum_{nn'} \sum_b \sum_i B_{L_i} \right]_{\text{within } 2\Delta\omega^*} \quad (10)$$

(vibrational bands) (band branches) (lines in each branch)

Assuming that the detector has essentially a flat response over $2\Delta\omega^*$, B/X may be related to the detector signal voltage through the expression

$$\frac{V}{X} \propto \frac{1}{X} \int \int B d\Omega dA = \frac{K'_r}{X} \mathcal{F} \quad (11)$$

where the integration is to be extended over the solid angle and the effective area subtended by the exit optics, K'_r is the overall response of the detection-recording system (signal voltage output/watt of light input) which must be determined by calibration, and \mathcal{F} is the total radiant flux passed by the monochromator. If the detector response varies appreciably over $2\Delta\omega^*$, the right-hand side of Eq. 9 should be multiplied by the relative spectral response of the detector at ω_i .

Combining Eqs. 9, 10 and 11 yields the result

$$\frac{V}{X} = K_r \frac{16\pi^3 c}{3k} \frac{|R_{e\ell}|^2}{TQ} \left[\sum_{nn'} |p_{nn'}|^2 \sum_b \sum_i \omega_i^4 [\exp(-E_{u_i}/kT)] |p_{kk'}|^2 g_{\omega_i} \right]_{2\Delta\omega^*} \quad (12)$$

where $K_r = K'_r / \Delta\Omega A_{\text{eff}}$, and $\Delta\Omega$ and A_{eff} are the solid angles and effective areas subtended by the exit optics, respectively.

Equation 12 is similar to Eq. 1 but has been modified to account for contributions from all of the bands passed by the monochromator and is expressed in terms of the voltage response and absolute calibration of the detection system. It should be noted that Eq. 12 may be used to relate the measured signal voltage from an emission experiment to the electronic moment $|R_{e\ell}|^2$ through the absolute calibration factor K_r since the other terms appearing in Eq. 12 are calculable. The absorption electronic f-number for the band system is related to $|R_{e\ell}|^2$ by the expression

$$(f_{\ell \rightarrow u})_{e\ell} \simeq \frac{8\pi^2 m_e c}{3he^2} \bar{\omega}_{0,0} |R_{e\ell}|^2 \quad (13)$$

The gas temperature is thus defined implicitly by Eq. 12 for any given value of optical depth. It is important to note that any errors in the shock-tube parameters (i.e., the pressure, concentrations, velocity, etc.) do not affect a temperature measurement as defined by Eq. 12, which is valid as long as the gas is optically thin, isothermal, and in statistical equilibrium.

As was indicated earlier in the present discussion, uncertainties in $|R_{el}|^2$ and the required absolute intensity calibration limit the accuracy with which Eq. 12 may be applied to a shock tube temperature measurement. These problems may, however, be circumvented by measuring the ratio of the voltage signals from two spectral regions identified by the subscripts 1 and 2, respectively, belonging to the same band system, viz.,

$$\frac{V_1/X}{V_2/X} = \frac{K_{r1}}{K_{r2}} \frac{\left[\sum_{nn'} |p_{nn'}|^2 \sum_b \sum_i \omega_i^4 \left[\exp(-E_{u_i}/kT) \right] |p_{kk'}|_i^2 g_{\omega_i} \right]_{2\Delta\omega^*_1}}{\left[\sum_{nn'} |p_{nn'}|^2 \sum_b \sum_i \omega_i^4 \left[\exp(-E_{u_i}/kT) \right] |p_{kk'}|_i^2 g_{\omega_i} \right]_{2\Delta\omega^*_2}} \quad (14)$$

Here the $|R_{el}|^2$ term does not appear since it is the same for both regions and it is, therefore, only necessary to perform the appropriate summations and to determine the relative sensitivities of the two detection systems, which is experimentally much easier to do than is the absolute calibration. Equation 14 may be written in the convenient form

$$\frac{V_1/X}{V_2/X} \frac{K_{r2}}{K_{r1}} = \frac{\left[\sum_{nn'} |p_{nn'}|^2 f_1(T)_{nn'} \right]_{2\Delta\omega^*_1}}{\left[\sum_{nn'} |p_{nn'}|^2 f_2(T)_{nn'} \right]_{2\Delta\omega^*_2}} = \phi(T) \quad (15)$$

where $f_1(T)_{nn'}$, and $f_2(T)_{nn'}$, represent the calculated double sums appearing in the numerator and denominator of Eq. 14, respectively; $\phi(T)$ then represents the calculated functional relationship which defines implicitly the gas temperature in terms of the voltage increases per unit optical depth for the two spectral regions observed.

III. NUMERICAL CALCULATIONS FOR OH

Detailed calculations for the OH bands were performed on an IBM 7090,* using the data of Dieke and Crosswhite⁽²⁴⁾ for the relative rotational transition probabilities, line locations, and energy levels. The slit function was assumed to be an isosceles triangle centered at ω_0 and normalized to a peak of 1.0, as shown in Fig. 1. The wavenumber interval $2\Delta\omega^*$ was chosen to be 1049 cm^{-1} , which corresponds to 100A at 3100A near the band head of the OH $^2\Sigma \rightarrow ^2\Pi$ system. Since the dispersion of a monochromator changes with wavenumber, the assumption of a constant value for $2\Delta\omega^*$ corresponds to a varying slit width as the wavenumber setting is changed. For the specified calculations, the detector overall response factor, K_r , changes linearly with slit width, which must be accounted for in the experiment. This problem is discussed further in the section on experimental facilities.

* Appreciation is expressed to Dr. R. Hickling for programming the required summations and to the Western Data Processing Center of U. C. L. A. where the machine computations were performed.

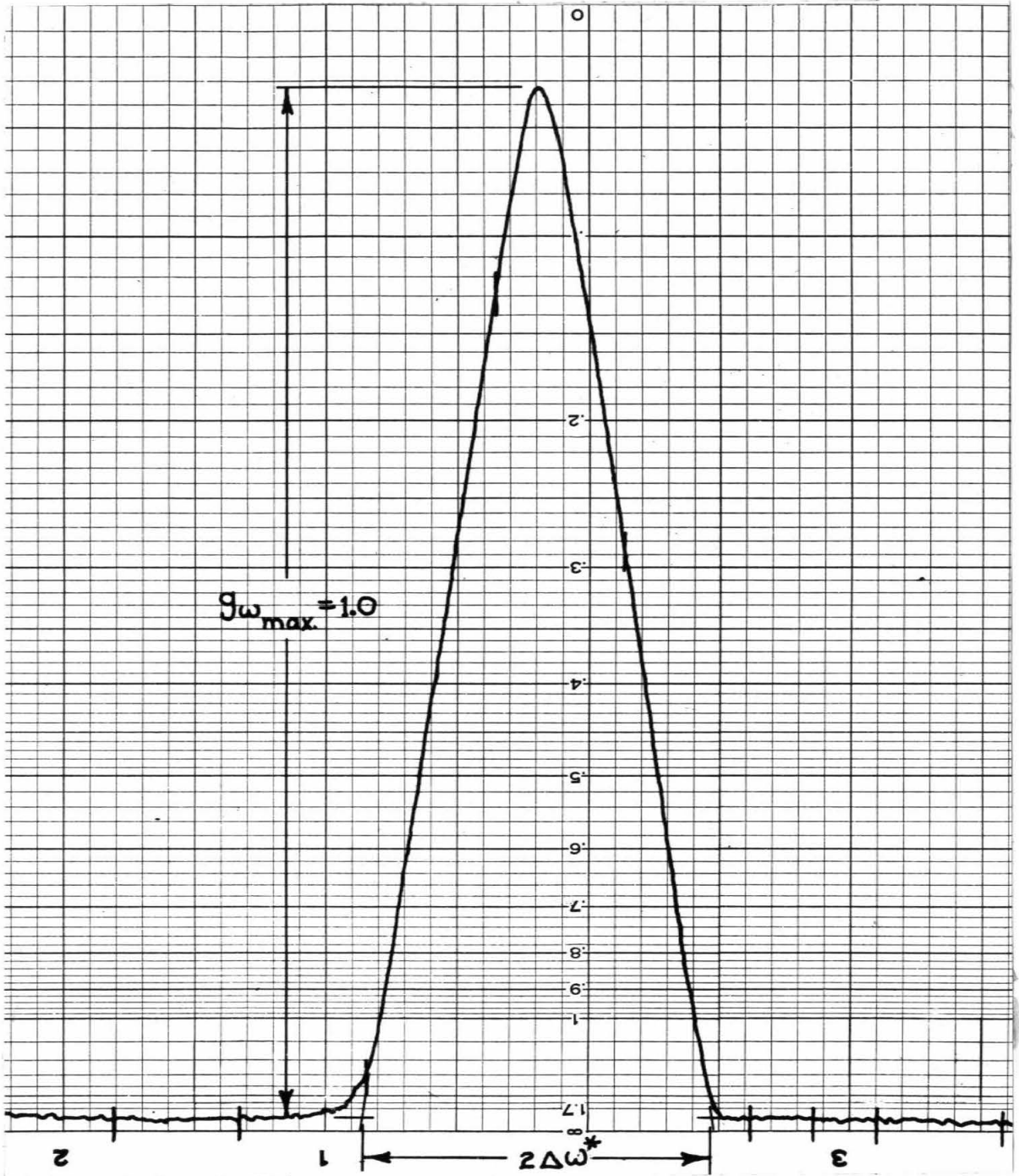


Fig. 1. The slit function for monochromator no. 1 as determined by scanning the 3341.48 Hg line with a thermocouple detector; monochromator slit width = 1.0 mm.

For the numerical calculations, the functions $f_j(T)_{nn'}$ ($j=1$ or 2), which are defined by the double summation in Eq. 14, were normalized by dividing by the term

$$F(T)^*_{(0,0)} = \left[\sum_b \sum_i \omega_i^4 [\exp(-E_{u_i}/kT)] |p_{kk'}|_i^2 \right]_{(0,0)} .$$

This quantity represents the upper bound on the $f_j(T)_{(0,0)}$ using a wide rectangular slit function. The variation of $F(T)^*_{(0,0)}$ with temperature is shown in Fig. 2 which thus affords an approximate measure of the relative intensity of the $(0,0)$ -band at different temperatures.

The term

$$\left[\sum_b \sum_i \omega_i^4 [\exp(-E_{u_i}/kT)] |p_{kk'}|_i^2 g_{\omega_i} \right]_{2\Delta\omega^*_j}$$

$$F_j(T)_{nn'} = \frac{\left[\sum_b \sum_i \omega_i^4 [\exp(-E_{u_i}/kT)] |p_{kk'}|_i^2 \right]_{2\Delta\omega^*_j}}{\left[\sum_b \sum_i \omega_i^4 [\exp(-E_{u_i}/kT)] |p_{kk'}|_i^2 \right]_{(0,0)}} \quad (j=1 \text{ or } 2) \quad (16)$$

replaces $f_j(T)_{nn'}$ in Eq. 15, which becomes now

$$\phi(T) = \frac{\left[\sum_{nn'} |p_{nn'}|^2 F_1(T)_{nn'} \right]_{\omega_{o_1}}}{\left[\sum_{nn'} |p_{nn'}|^2 F_2(T)_{nn'} \right]_{\omega_{o_2}}} . \quad (17)$$

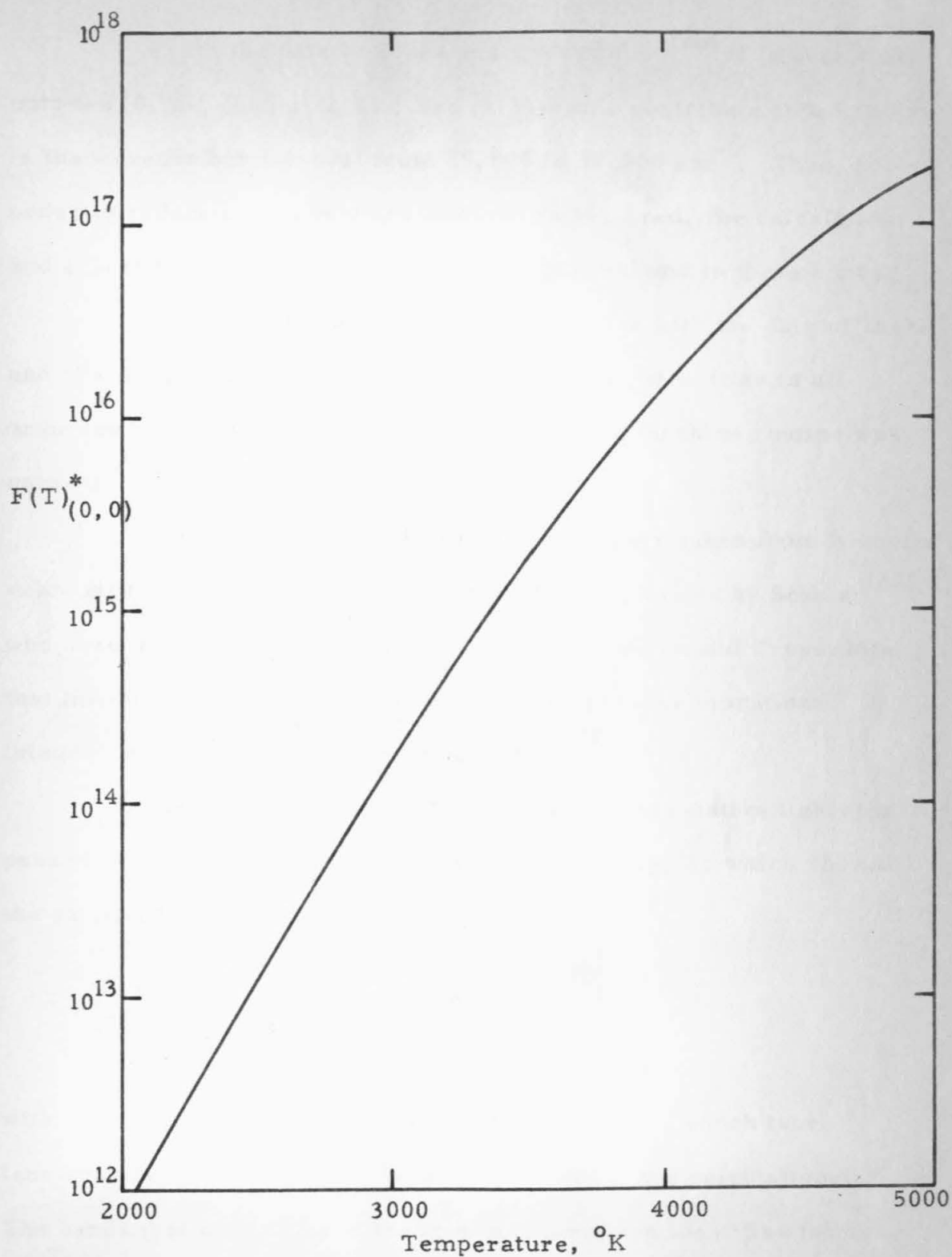


Fig. 2. The relative intensity of the (0,0)-band at various temperatures (the plotted data correspond to the use of a wide, rectangular slit function).

From the data of Dieke and Crosswhite,⁽²⁴⁾ it is seen that only the (0,0)-, (1,1)-, (2,2)-, and (3,3)-bands contribute appreciably in the wavenumber interval from 29,000 to 33,000 cm^{-1} . Thus, in order to reduce the amount of computation required, the calculations and experiments were restricted to this interval and to these bands.

Comparisons of the 7090 computations with the data of Dieke and Crosswhite were made for the relative line intensities in all branches of all bands in order to verify that the machine routine was correct.

Vibrational overlap integral values were taken from Nicholls' calculations,⁽²³⁾ which are in agreement with estimates by Schuler⁽²⁵⁾ who used unpublished band intensity data from Dieke and Crosswhite that involved slight revisions of some of the relative vibrational intensities reported in their original work.⁽²⁴⁾

The effect of wavenumber setting on the relative light flux passed by the monochromators may be seen in Fig. 3, which shows the variation of the intensity term

$$\left[\sum_{nn'} |P_{nn'}|^2 F_j^{(T)}(n, n') \right]_{\omega_j}$$

with wavenumber at constant temperature. Typical shock tube temperatures of 3000 to 5000^oK were chosen for the calculations. The bands that contribute to the intensity term are identified for the appropriate wavenumber intervals.

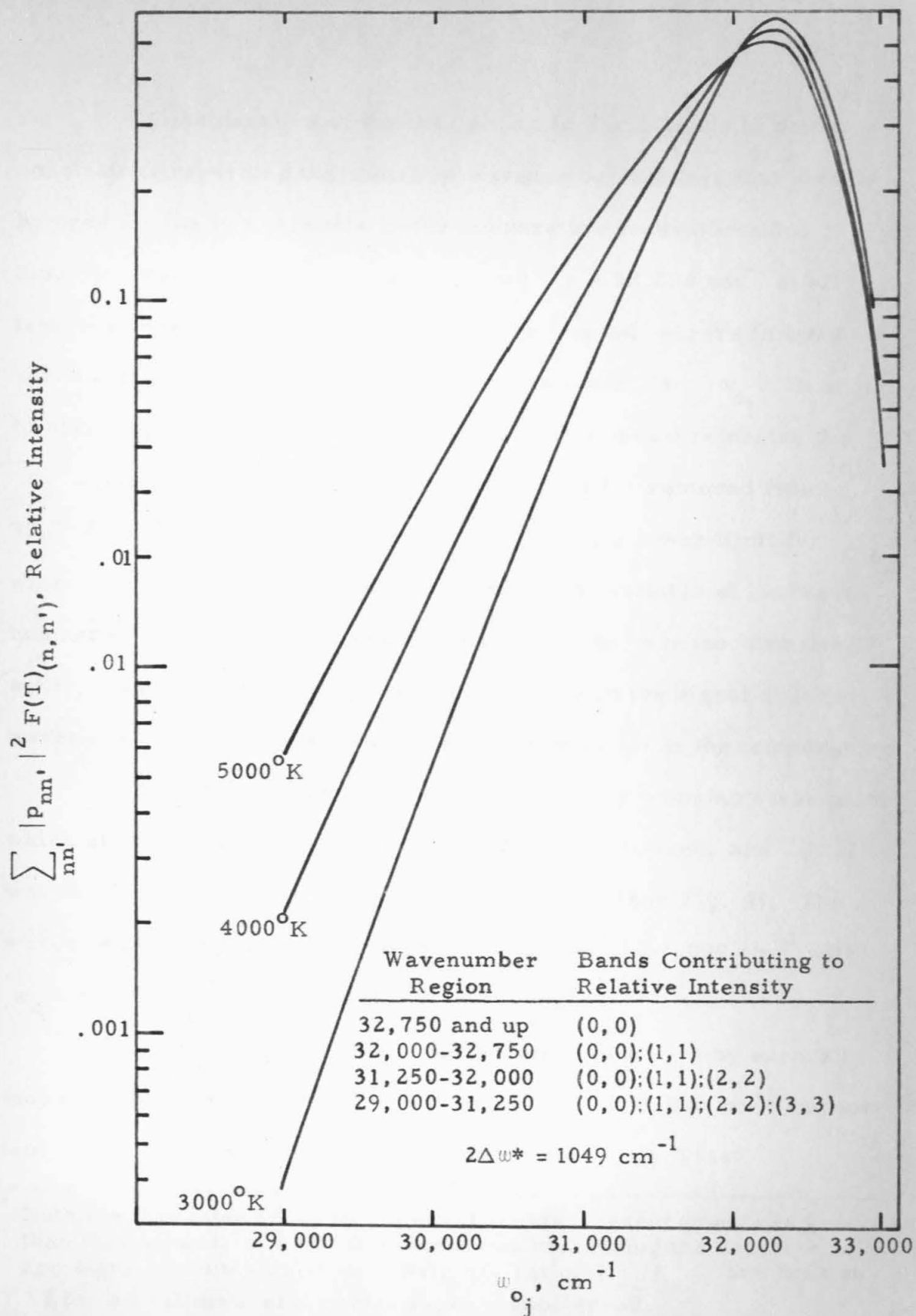


Fig. 3. Relative intensity vs. wavenumber setting for a monochromator with $2\Delta\omega^* = 1049 \text{ cm}^{-1}$ and a triangular slit function.

Consideration of the data shown in Fig.3 leads to some conclusions regarding the choice of wavenumber settings that should be used for the two channels in the temperature measurements. Since the maximum intensity occurs near $\omega_0 = 32,250 \text{ cm}^{-1}$ at all temperatures and is relatively insensitive to small errors in monochromator setting, this value is an obvious choice for ω_{o1} . In order to obtain optimal sensitivity in the temperature measurements, the ω_{o2} setting for the other channel should be as far removed from $32,250 \text{ cm}^{-1}$ as possible. There is, of course, a lower limit for ω_{o2} which is governed by the signal-to-noise ratio available at low wavenumbers. Also, it is seen that for a given error in monochromator setting, a greater percentage variation occurs in the signal at lower wavenumbers, thus leading to a greater uncertainty in the temperature.

In view of these factors, a choice of wavenumbers was made which allowed reasonable signal strengths to be attained, and $\phi(T)$ was then calculated as a function of temperature (see Fig. 4). The wavenumber range chosen extended from $31,000$ to $32,000 \text{ cm}^{-1}$ with $\omega_{o1} = 32,250 \text{ cm}^{-1}$ for all cases.

The maximum error in temperature produced by errors in monochromator settings alone* occurs for $\omega_{o2} = 31,000 \text{ cm}^{-1}$ and low temperatures ($\sim 3000^\circ\text{K}$). The relative error in $\phi(T)$ is

* Note that the total error in the experimental measurements is greater than this because of additional errors in measuring the detector voltage signals and the relative sensitivity ratio, K_{r2}/K_{r1} . See Section VI for an estimate of the total experimental error.

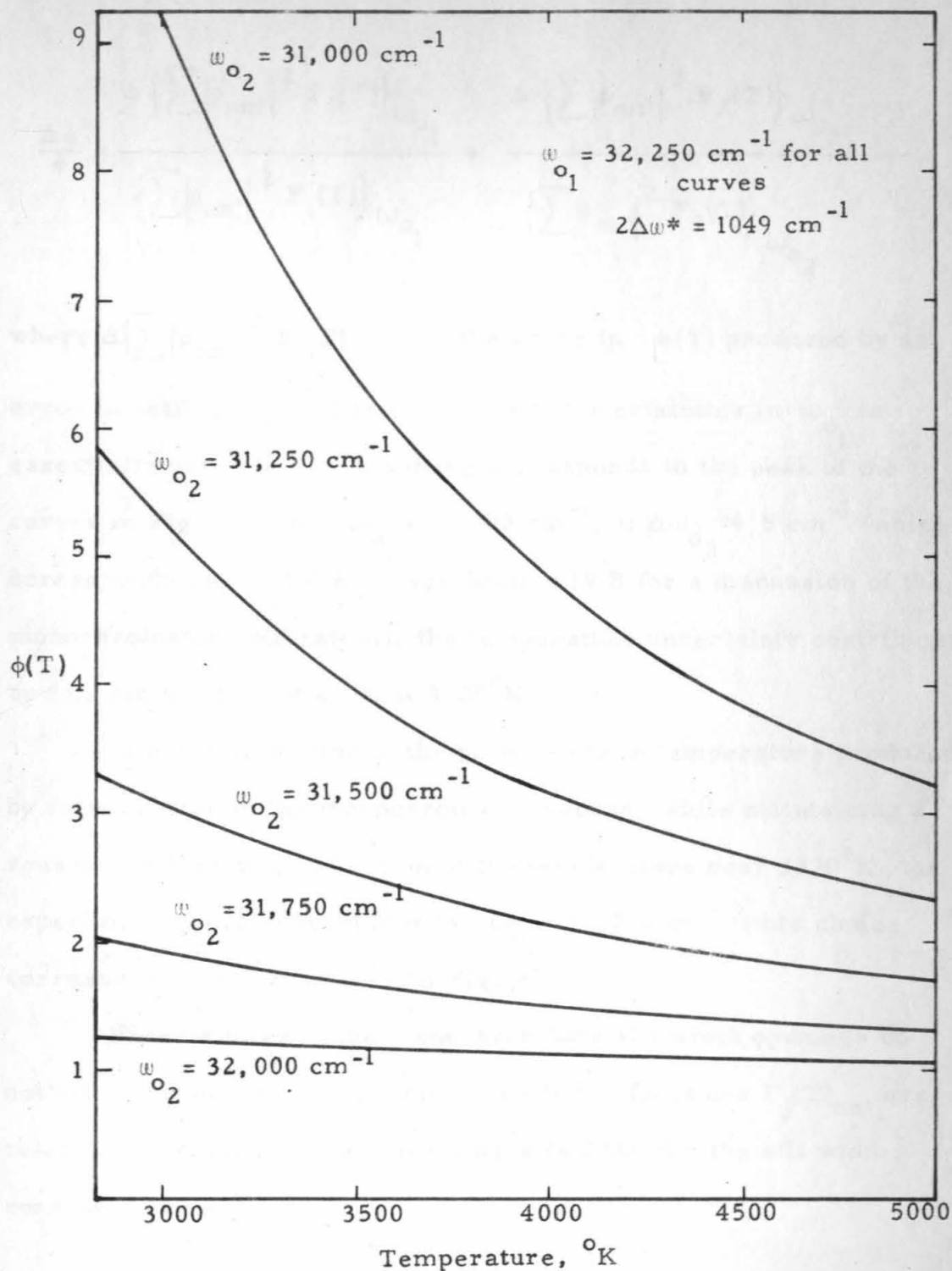


Fig. 4. The intensity ratio, $\phi(T)$, as a function of temperature for ω_{o_2} from 31,000 to 32,000 cm^{-1} .

$$\frac{\Delta\phi}{\phi} = \frac{\Delta \left\{ \sum |p_{nn'}|^2 F_1(T) \right\}_{\omega_{o_1}}}{\left\{ \sum |p_{nn'}|^2 F_1(T) \right\}_{\omega_{o_1}}} + \frac{\Delta \left\{ \sum |p_{nn'}|^2 F_2(T) \right\}_{\omega_{o_2}}}{\left\{ \sum |p_{nn'}|^2 F_2(T) \right\}_{\omega_{o_2}}}$$

where $\Delta \left\{ \sum |p_{nn'}|^2 F_j(T) \right\}_{\omega_{o_j}}$ is the error in $\phi(T)$ produced by an error in setting ω_{o_j} . The error due to uncertainties in ω_{o_1} is essentially zero since this setting corresponds to the peak of the curves in Fig. 3. For $\omega_{o_2} = 31,000 \text{ cm}^{-1}$, if $\Delta\omega_{o_2} \approx 5 \text{ cm}^{-1}$ (which corresponds to about $\frac{1}{2} \text{ \AA}$ — see Section IV B for a discussion of the monochromator calibration), the temperature uncertainty contributed by this factor is $\Delta T \approx 25^\circ \text{K}$ at 3000°K .

In order to minimize the uncertainty in temperature produced by inaccuracies in the monochromator setting, while maintaining a reasonably sensitive indication of the temperature near 3500°K , the experiments were conducted with $\omega_{o_2} = 31,000 \text{ cm}^{-1}$ (this choice corresponds to the top curve in Fig. 4).

Uncertainties in the monochromator slit width openings do not affect the accuracy appreciably since the functions $F_j(T)_{nn'}$ are relatively insensitive to small changes in $2\Delta\omega^*$ for the slit width considered here.

IV. EXPERIMENTAL FACILITIES

A schematic diagram of the essential components of the apparatus (except for the gas-handling equipment) is shown in Fig. 5. An overall view of the apparatus is shown in Fig. 6. The gas-handling system is represented schematically in Fig. 8.

A. The Shock Tube and Associated Measuring Apparatus

The shock tube was of conventional, closed-tube design with a 6 foot low-pressure test section and a 5 foot high-pressure driver section separated by Mylar plastic diaphragms.* The tube was fabricated from seamless steel tubing honed to a uniform diameter ($3.079 \pm .001$ inches) with a surface finish of better than RMS 20. The test section vacuum before loading with test gas was between 0.1 and 0.2 microns with an indicated leak rate of 0.01 to 0.1 microns per minute. A 1/4 inch thick General Electric type 101 quartz window was placed in the center of the end plate; this window had a 1 cm aperture opening for axial observations. A 3/16 inch thick type 101 quartz window with a 1 cm aperture was located 1.80 inches from the end plate for auxiliary observations normal to the tube axis. Accommodations for thin film gages used for shock-velocity measurements were provided in three stations, thus allowing an estimate of shock speed attenuation to be made. The circuitry for the velocity measurement

* This shock tube is a modification of one constructed under Contract No. AF 18(603)-2, AFOSR, ARDC and used also for work under Contract No. AF 49(638)-984 AFOSR, ARDC (see Ref. 4).

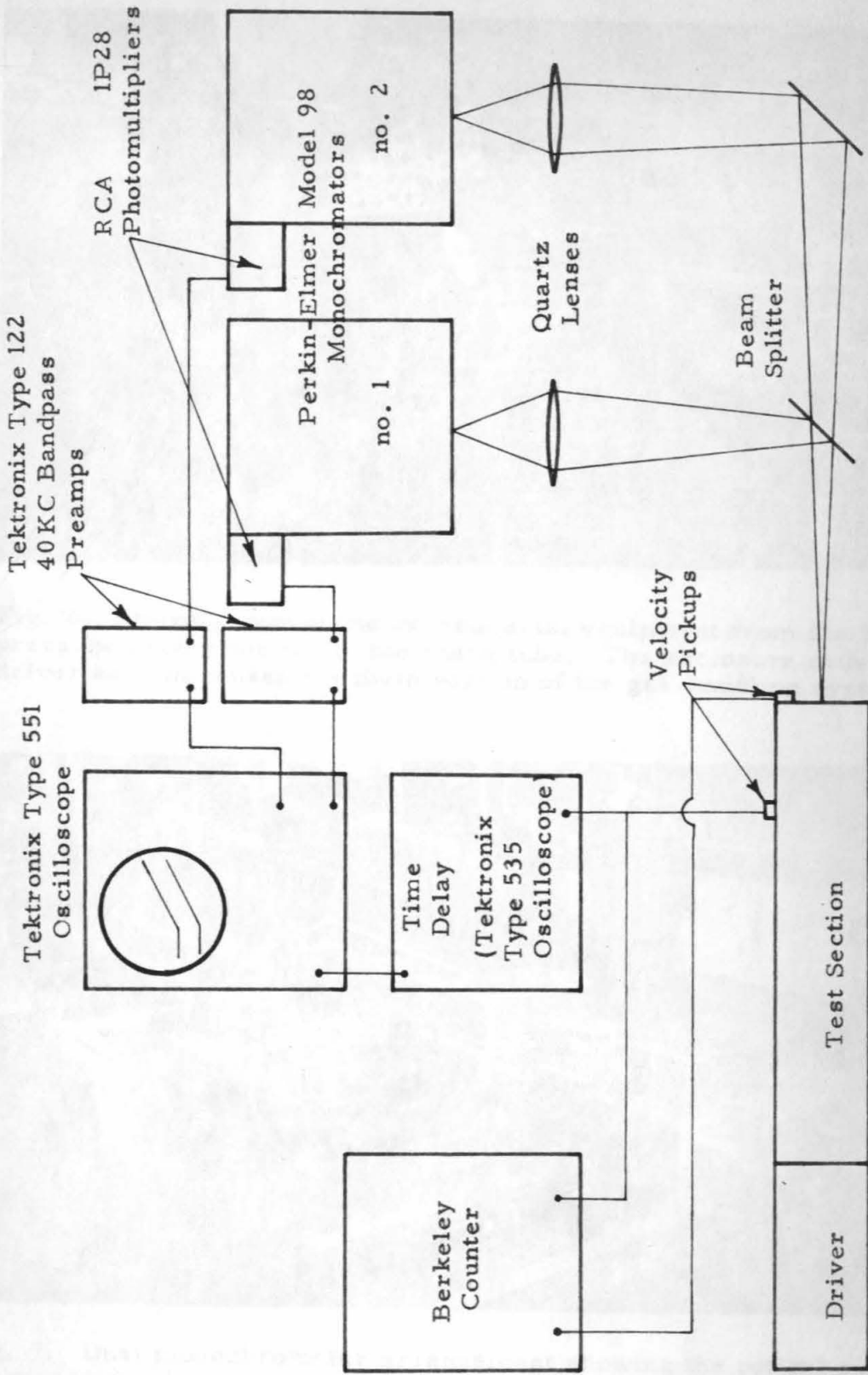


Fig. 5. Schematic diagram of the experimental equipment.

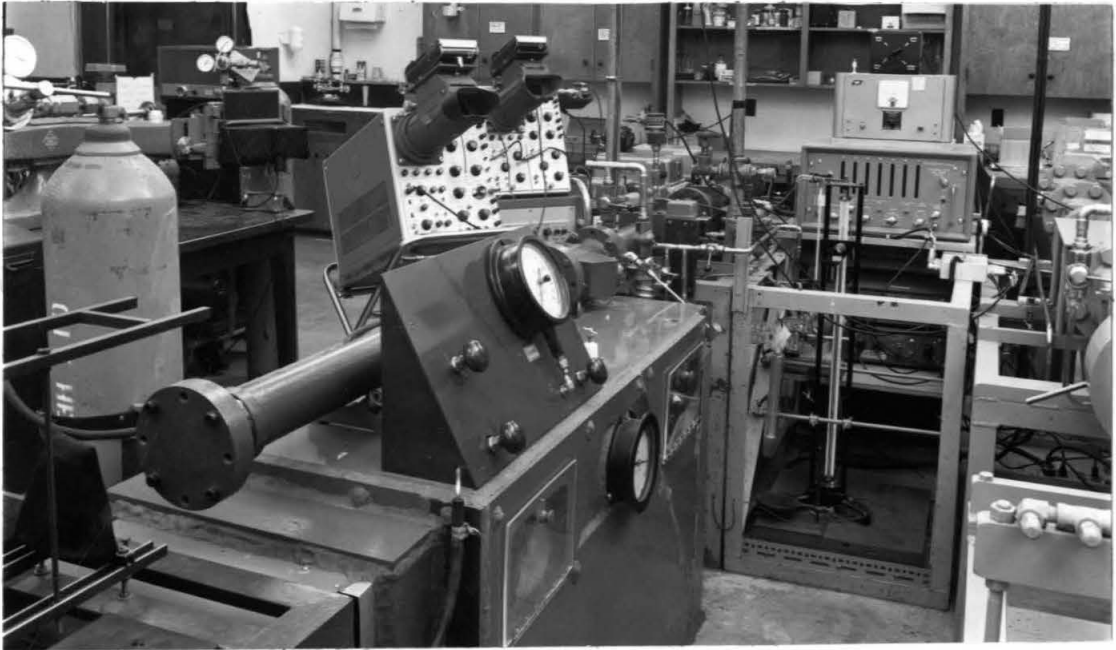


Fig. 6. Overall view of the experimental equipment from the high pressure driver section of the shock tube. The enclosure under the driver section houses the main portion of the gas-handling system.



Fig. 7. Dual monochromator arrangement showing the optical system for viewing emission from the shock tube in the axial direction.

system was essentially the same as that described in Ref. 26.

B. The Optical System

Isolation of the required spectral intervals of the emission from the hot gas was achieved by the use of two Perkin-Elmer Model 98 monochromators, one equipped with a fused silica (quartz) prism and the other with a lithium fluoride prism. A view of the dual monochromator arrangement is shown in Fig. 7. A half-aluminized thin quartz disc served as a beam splitter in the path of the emission from the shock-tube end window (see Fig. 5), and quartz lenses were used to focus the image of the end window on the monochromator entrance slits. Apertures in front of the quartz lenses limited the optical systems to observations in a narrow core of gas in the center of the shock tube about 1 cm in diameter and essentially cylindrical in shape, with an included divergence angle of less than $\tan^{-1} (.04)$. Thus, side wall boundary layer effects and reflections from the inside of the shock tube walls do not affect the measurement and the volume of gas emitting radiation into the optical system grows linearly with time as the reflected shock moves up the tube. Viewing emission axially behind the reflected shock allows an experimental check to be made on the assumptions that the gas is transparent and in equilibrium if the axial emission is linear with time. Corning 7-54 color filters were installed in the optical path to reduce the possibility of internal light scattering in the monochromators from wavelengths outside the ultraviolet region of the spectrum.

Quartz condensing lenses were used to focus the light from the exit slits of the monochromators onto RCA 1P28 photomultipliers. Regulated power supplies maintained constant high voltage (~ 500 V. D. C.) for the voltage divider network of the photomultiplier (see Ref. 26 for a description of the network). The time response of the load circuitry of the photomultipliers was $\sim 0.2 \mu\text{s}$, but Tektronix type 122 preamplifiers set at 40 KC band pass for noise reduction limited the overall electronic response to about $5 \mu\text{s}$. This response proved adequate since the signal from the emission behind the reflected shock increased linearly on a time scale much longer than $5 \mu\text{s}$. The signals were recorded by photographing the traces on a Tektronix type 551 dual-beam oscilloscope. The linearity of the responses of the detection systems to varying levels of incident light was checked by using emission from a tungsten lamp focused into both of the optical systems.

Monochromator wave length calibrations were performed by utilizing various spectral lines from gas discharge tubes. The reproducibility and accuracy of the settings was about $1/3\text{\AA}$ with spot rechecks, just prior to each experiment, maintaining this accuracy. The slit function responses were determined from thermocouple signals obtained by scanning various lines of a low-pressure Hg lamp (see Fig. 1 for a typical slit function).

C. The Gas-Handling System

The OH was generated by the dissociation of water vapor diluted with argon in the shock tube. In order to achieve the transparency required by the theoretical considerations, it was necessary to go to very dilute initial water vapor concentrations, namely 0.3 to 0.5%. Mixtures of argon and water vapor prepared in external mixing systems, however, exhibit excessive preferential adsorption of the water vapor on the walls of the gas-handling equipment and the shock tube during the bleed-in procedure.⁽²⁷⁾ The extent of this surface adsorption of the water vapor may be as high as 30 to 50% of the initial concentration value; these values were established as the result of measurements on the shock tube used for this study (before honing) by analyzing samples of test gas drawn out through the gas inlet lines after the gas had been in the shock tube from 5 to 10 minutes. The initial concentrations for these measurements were $\sim 3\%$ H_2O and the test gas pressures were 50 mm Hg. In addition to the uncertainties of overall concentration introduced by the adsorption, concentration gradients may be set up within the shock tube so that samples drawn from the tube just before firing may not be representative of those in the region of observation.

While it is not required to know the initial concentration precisely for the spectroscopic temperature measurement (compare Eq. 12), the calculated equilibrium temperature is sensitive to the initial water vapor since H_2O has a relatively high heat of dissociation.

Attempts were made to overcome the adsorption difficulties by conditioning the shock tube walls to an adsorption equilibrium state. This was done by utilizing the vapor pressure above bulbs of liquid water to cause diffusion mixing of the water vapor and argon in the test section; the results were erratic, however. Repeated flushing cycles with a mixture left in the tube for 10 minutes, and then pumped down to about 1-2 mm of Hg before bleeding in a fresh mixture, also proved unsatisfactory.

A successful procedure was arrived at through use of a continuous flushing operation employing the system shown in Fig. 8. This system used a regulated argon flow, bubbled continuously through a series of bulbs containing degassed water. A flow meter was used to monitor the approximate flow rates, regulation being achieved by bellows valves at the inlet and outlet of the flow system. A cold trap prevented the water vapor from contaminating the vacuum pump oil. A small air conditioning unit was used to recirculate air within an insulated enclosure, allowing controlled temperatures of 0 to 25^oC to be maintained in the mixing system. Since the ratio of vapor pressure above the liquid water compared to the total mixing pressure determined the water vapor concentration, the cooling system allowed low percentage concentrations to be obtained without dangerously overpressurizing the associated glassware.

To provide an opening in the shock tube for the flushing procedure while maintaining a flat end wall for the reflected shock experiments, a recessed valve was devised and is shown in Fig. 9.

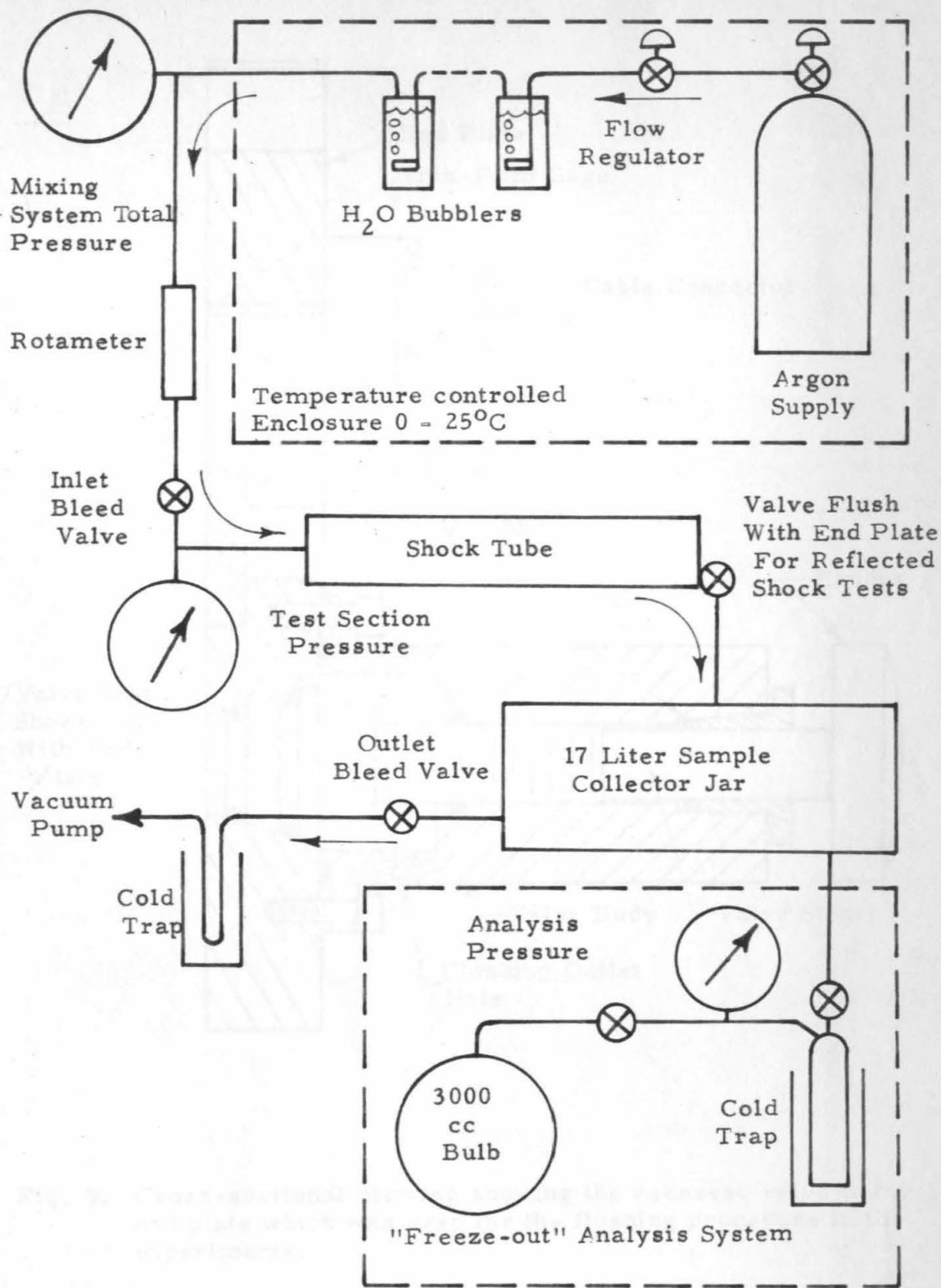


Fig. 8. Schematic representation of the gas-handling and flushing system for the argon-water vapor test gas mixtures.

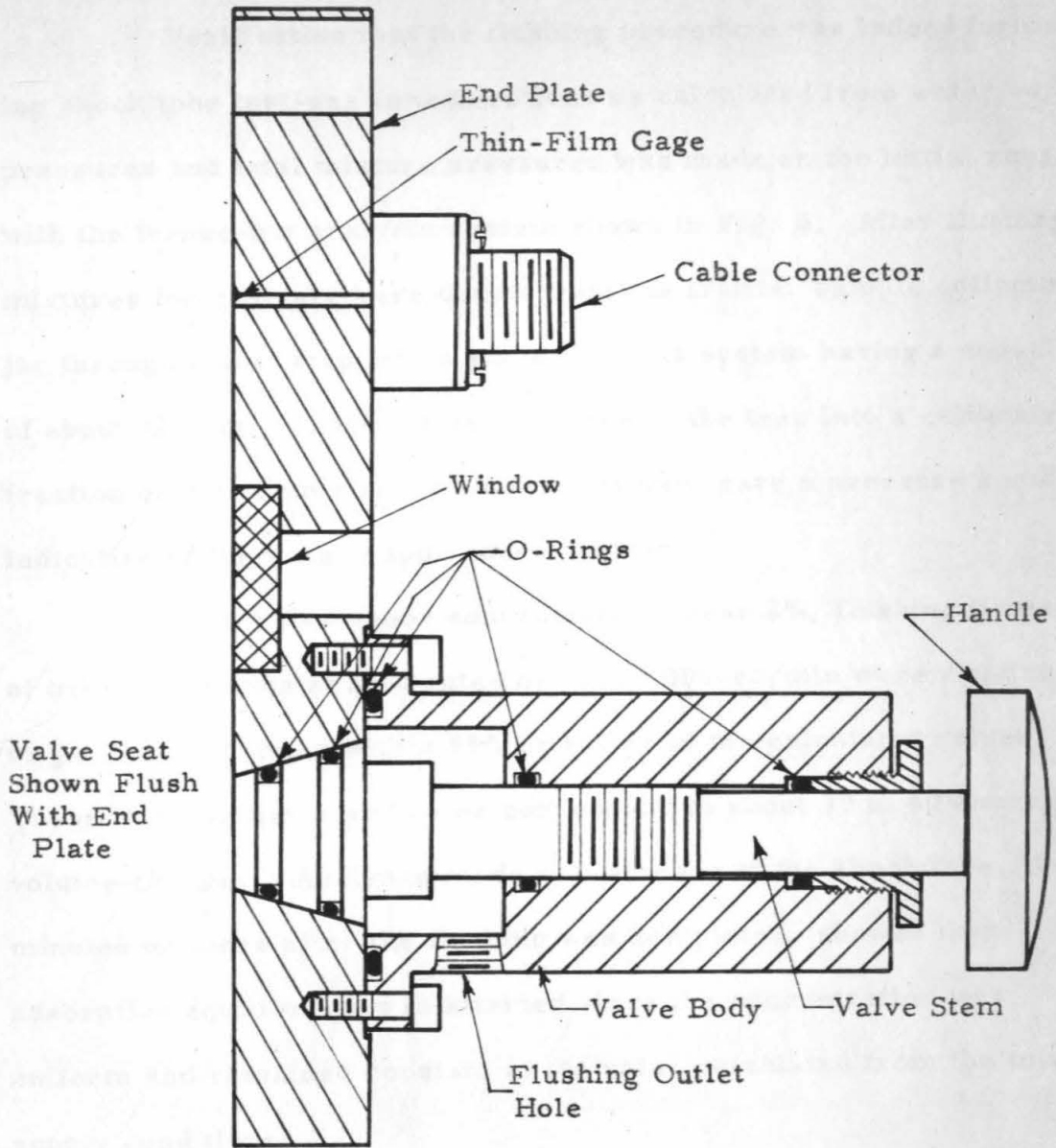


Fig. 9. Cross-sectional drawing showing the recessed valve in the end plate which was used for the flushing procedure in the experiments.

Verification that the flushing procedure was indeed furnishing shock tube test-gas concentrations as calculated from water vapor pressures and total mixture pressures was made on the initial runs with the freeze-out analysis system shown in Fig. 8. After flushing, mixtures for analysis were drawn from the 17-liter sample collector jar through a cold trap into a glass analysis system having a capacity of about 3200 cc. Evaporation of the ice in the trap into a calibrated fraction of the volume of the analysis system gave a pressure reading indicative of the water vapor concentration.

With water vapor concentrations near 3%, flushing times of over 30 minutes at flow rates of about 1000-cc/min were required to get concentrations within 95% or better of the calculated values. These flushing times and rates correspond to about 30 to 40 shock tube volume changes. Analyses made at both ends of the shock tube, 10 minutes or more after the flushing was completed, showed that adsorption equilibrium was attained since the concentration was uniform and remained constant at the value calculated from the mixing supply conditions.

The flushing procedure was used before making quantitative shock tube measurements. Thermocouple measurements in the flow system showed that the mixture was essentially at room temperature within the shock tube.

Although the water vapor adsorbed on the walls and end

plate will tend to diffuse into the test gas region, an upper limit to the diffusion time required for this process is given by the relation

$$\tau_D \sim \frac{L^2}{D_{12}}$$

where L is a characteristic diffusion length (e.g., the shock tube radius) and D_{12} is the binary diffusion coefficient. Estimates from data in Ref. 28 indicate that $\tau_D \sim 4$ seconds. Therefore, the diffusion effects should be restricted to the boundary layers during the $200\mu\text{s}$ testing time available for the temperature measurements (see Fig. 11).

Impurity radiation levels observed from pure argon shots using the regular flushing procedure but without the water flasks were about 1/2% of the signal levels observed during the spectroscopic temperature measurements.

V. EXPERIMENTAL PROCEDURE

A. Determination of the Relative Intensity Ratio K_{r_2} / K_{r_1}

The ratio of relative sensitivities of the two optical systems, which is required for the data reduction, was obtained directly from shock tube experiments with both monochromators monitoring the same wavenumber setting ($32,250 \text{ cm}^{-1}$) and spectral interval, $2\Delta\omega^*$. The ratio of signal voltages for these shock tube calibration runs is the desired value of K_{r_2} / K_{r_1} . The solid angles of the optical systems and geometrical slit widths do not have to be identical since these are included in the K_r factors (see Eq. 11). However, in the calibration

experiment, the effective spectral distribution of the light observed by the instruments must be the same (i. e., the same slit function as well as the same wavelength settings must be used) since the detectors must be calibrated relative to the same incident light flux.

Since the wavenumbers ω_{o_1} and ω_{o_2} used for the experiment are within 100A, no corrections were required to account for changes in transmission and solid angles of the associated optics in changing the setting of monochromator no. 2 from $31,000 \text{ cm}^{-1}$ to $32,250 \text{ cm}^{-1}$ for the calibration. Because of the variation of dispersion of the prism with wavenumber, the slit width had to be adjusted slightly as the setting of monochromator no. 2 was changed from ω_{o_2} to ω_{o_1} for the calibration. This change is, however, unimportant because the spectral range covered is very small.

The calibration runs were performed after about three temperature measurements or when fresh batteries were installed in the pre-amplifiers. Experiments showed that the resulting K_{r_2}/K_{r_1} data were reproducible within about a 3% range.

B. Thermodynamic Properties of the Gas Behind the Shock Wave

A comparison of the measured spectroscopic temperature with the equilibrium temperature was made by using data derived from an IBM 7090 machine program at the Aerospace Corporation in

Los Angeles.* The value of $\Delta H_f^0 = +9.27$ kcal/mole for OH at 0°K was used in these calculations. (29)

All experiments were conducted with 50 mm Hg initial pressure and about 299°K initial temperature. The machine computations covered from 0 to 1.0% of water vapor in argon for incident shock velocities from 1.20 to 1.40 mm/ μs , which correspond to reflected shock temperatures of 3000 to 4200°K . A plot of the calculated results is shown in Fig. 10. Hand calculations and an independent machine computation at Los Alamos** were used to verify the Aerospace calculations. A recheck of the temperature calculations given in Ref. 4, showed these to be high in some cases by about 80 to 100°K .

Because of the low concentration of water vapor involved, the calculated equilibrium conditions behind the reflected shock are practically the same if either equilibrium or frozen conditions are assumed behind the incident shock wave.

VI. EXPERIMENTAL RESULTS

A typical oscilloscope record is shown in Fig. 11. The initial slopes of these records, together with the K_{r_2}/K_{r_1} calibration, permit determination of the spectroscopic temperature of the OH by utilizing the graph in Fig. 4. In Table 1, the results derived from a

* Grateful acknowledgement is made to Messrs. R. L. Wilkins, R. A. Hartunian, and H. J. Vale for use of the Aerospace program and machine time.

** Dr. G. L. Schott kindly performed extensive checks on the Los Alamos shock-wave program.

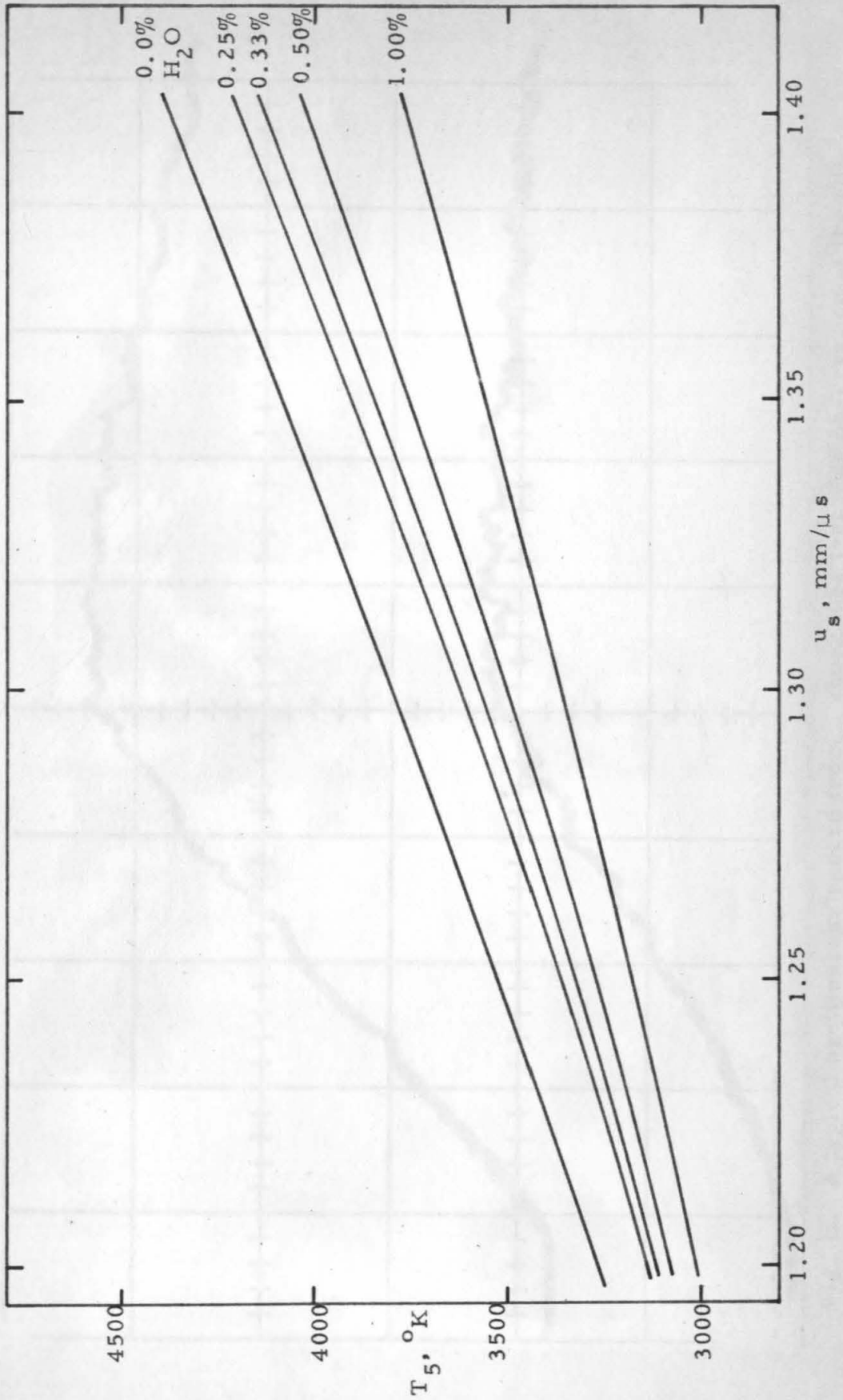


Fig. 10. The calculated equilibrium temperature T_5 behind the reflected shock as a function of incident shock velocity.

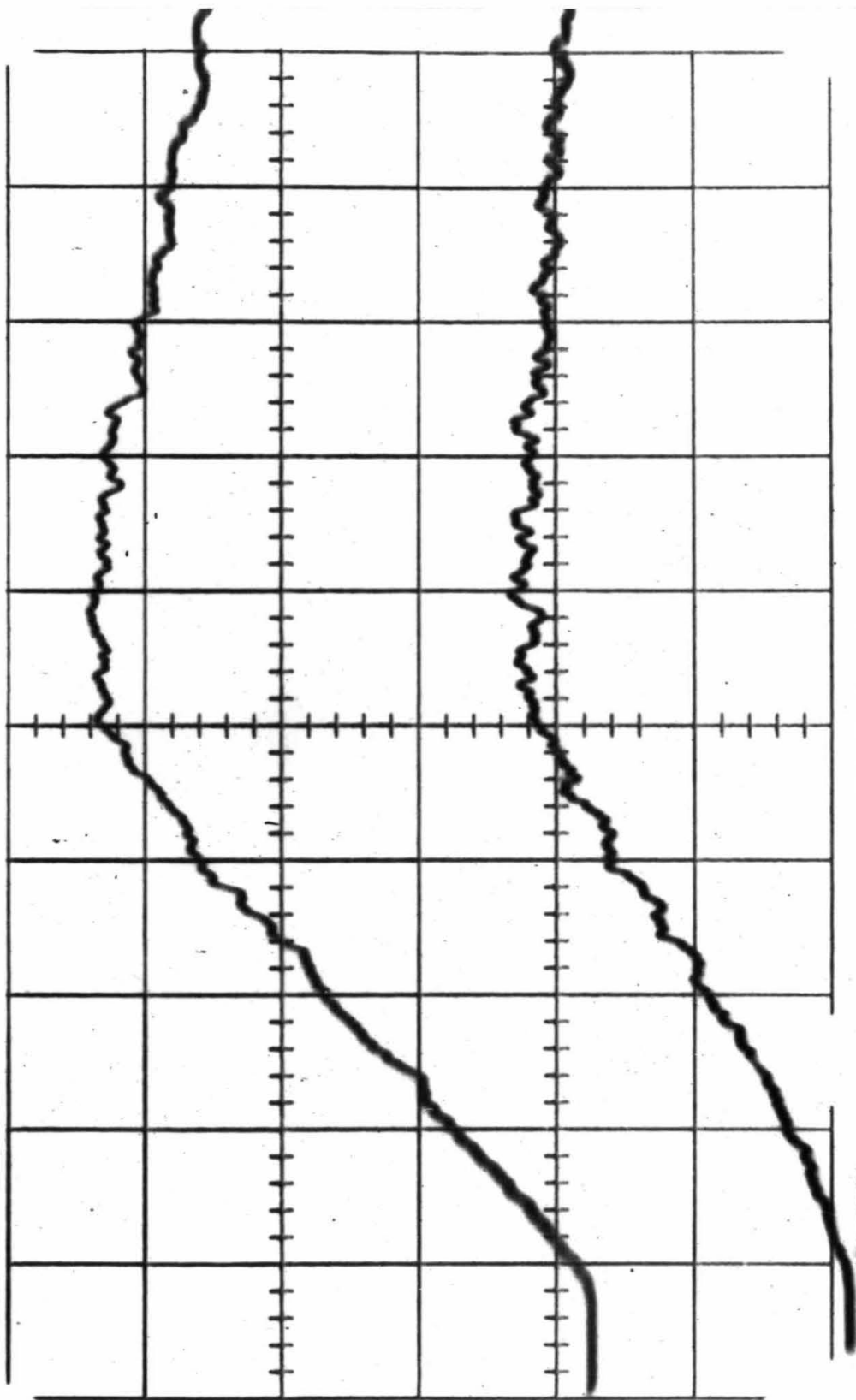


Fig. 11. A typical oscilloscope record from a shock tube test with observation of the OH emission in the axial direction behind the reflected shock wave. Sweep speed = $50 \mu\text{s}/\text{cm}$. The upper trace is for $32,250 \text{ cm}^{-1}$ at $10 \text{ mv}/\text{cm}$; the lower trace is for $31,000 \text{ cm}^{-1}$ at $5 \text{ mv}/\text{cm}$. The spectroscopic temperature is 3680°K and the calculated equilibrium temperature is 3620°K . Initial H_2O concentration is 0.30% .

TABLE I. Tabulation of experimental results.

Initial H ₂ O concentration (per cent)	Incident shock velocity (mm/ μ s)	Measured spectro- scopic temperature (^o K)	Calculated equilibrium temperature (^o K)	$\Delta T = T_{\text{spect}}$ $- T_{\text{equil}}$ (^o K)
0.50	1.314	3520	3583	-63
0.50	1.299	3550	3510	+40
0.30	1.329	3710	3775	-65
0.30	1.292	3710	3580	+130
0.30	1.299	3680	3620	+60
0.30	1.306	3685	3650	+35
0.29	1.303	3510	3630	-120
0.30	1.337	3800	3840	-40
0.30	1.281	3530	3510	+20
0.30	1.326	3740	3750	-10
0.30	1.299	3600	3615	-15
0.31	1.303	3580	3625	-45
0.29	1.299	3595	3625	-30
0.33	1.232	3385	3280	+105
0.33	1.246	3490	3350	+140
0.33	1.416	4250	4270	-20
0.33	1.314	3620	3690	-70

number of experiments are compared to the calculated equilibrium temperatures.

Figure 12 shows an oscilloscope signal from an experiment in which emission normal to the tube axis was observed from a 1 cm diameter window in the side wall at a distance of 1.80 inches from the end of the shock tube. This location corresponds to a time interval of about $70\mu\text{s}$ after the reflected shock leaves the end plate and thus is about in the middle of the $200\mu\text{s}$ testing time of the axial observations shown in Fig. 11.

The linear growth of intensity observed in the axial runs, coupled with the steady signal during the early part of the cross-tube observations at the window location 1.80 inches from the end wall, indicates that the gas is transparent, isothermal, and in thermal equilibrium during the time interval of $200\mu\text{s}$ required for the spectroscopic temperature measurements. Approximately 10^6 collisions occur between the OH and other species during the $200\mu\text{s}$ period.

A cross-tube observation at a second window location 5.80 inches from the end wall showed that the OH emission was reduced by more than a factor of 30 below the level of the cross-tube observations at the first window. The location of the second window corresponds to the point where the reflected shock is about $200\mu\text{s}$ from the end wall and suggests that the reflected shock interacts with the contact region

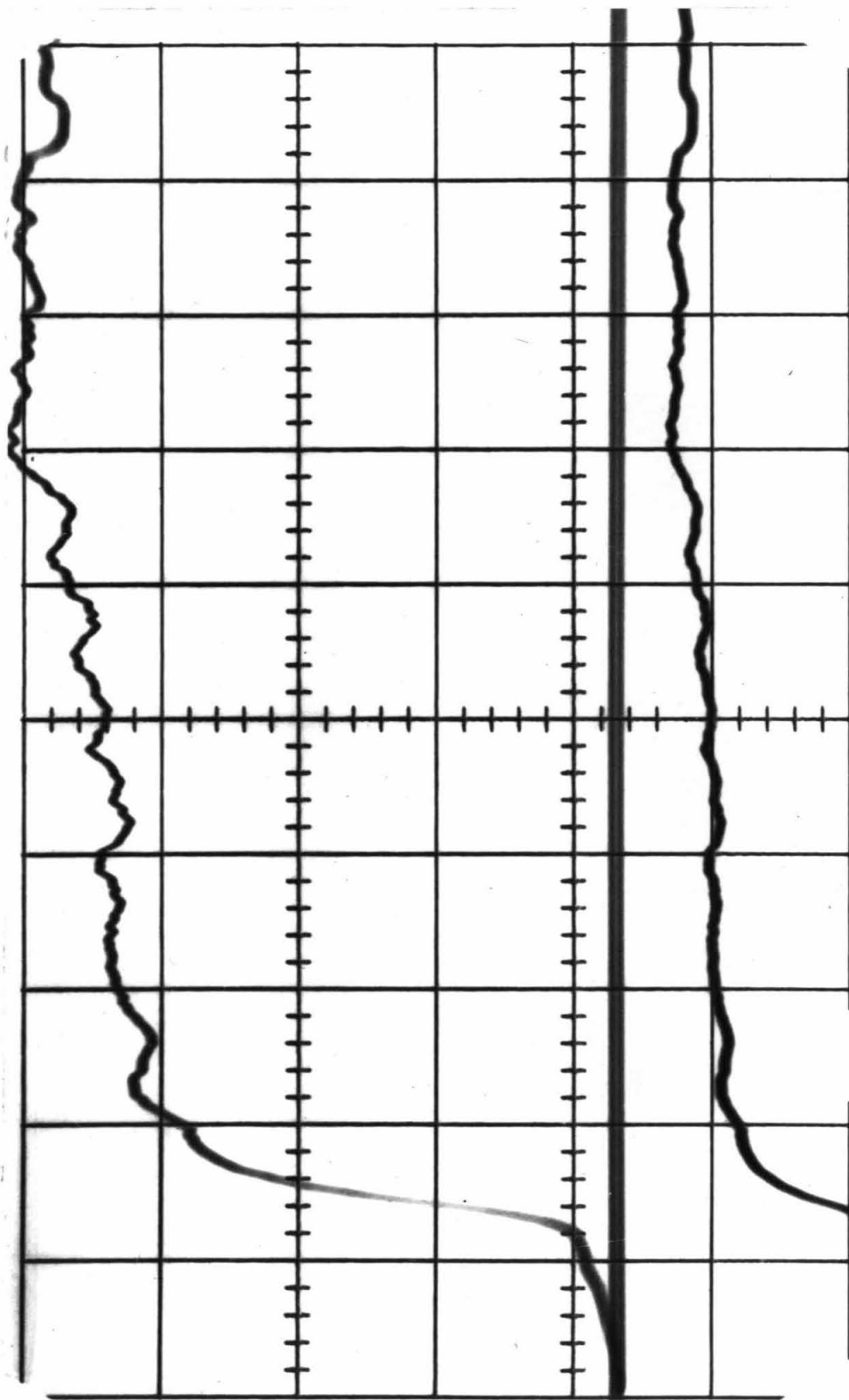


Fig. 12. Oscilloscope record of the OH emission behind the reflected shock viewed normal to the shock tube axis at 1.80 inches from the end wall. Sweep speed = $50 \mu\text{s}/\text{cm}$. Both traces are at $32,250 \text{ cm}^{-1}$; the upper trace gain is $20 \text{ mv}/\text{cm}$, the lower trace gain is $50 \text{ mv}/\text{cm}$. Initial H_2O concentration is 0.50%.

near that point and thus may explain the decay in intensity in the axial observations after about 200 μ s in Fig. 12.

A. Estimate of Accuracy

The estimated accuracy of the spectroscopic temperature measurements is about $\pm 75^\circ\text{K}$. Contributions to this total error come from (a) errors in monochromator settings, (b) errors in the K_{r_2}/K_{r_1} calibration, and (c) uncertainties in determining V_1/V_2 from oscilloscope records. The error due to uncertainties in the monochromator setting is about 25 to 30°K , as discussed in Section III (on Theoretical Considerations). The uncertainty in the K_{r_2}/K_{r_1} calibration was about 3%. From Fig. 4, it may be seen that this uncertainty in K_{r_2}/K_{r_1} produces about $\pm 30^\circ\text{K}$ uncertainty in the spectroscopic temperature. The initial slopes of the oscilloscope records could be determined to about 3% uncertainty, which leads to an uncertainty of about $\pm 30^\circ\text{K}$ in the measured temperature.

The comparison between the spectroscopic and equilibrium temperatures shown in Table 1 varies more than $\pm 75^\circ\text{K}$ in some cases, presumably because there are uncertainties in the shock-tube performance data (such as measured shock velocities and initial mixture temperatures). A $\pm 1\%$ variation in the measured shock velocity causes a variation of about $\pm 65^\circ\text{K}$ in the calculated reflected shock temperature, while a 2°C uncertainty in initial temperature causes a variation of about 25°K behind the reflected shock. Negligible errors in the reflected shock temperatures are introduced by fairly large

uncertainties (e.g., $\pm 5\%$ or more) in initial pressure because the temperature ratios across the shocks are not sensitive to this parameter.

B. Comparison with Other Experiments

In the previous shock tube temperature measurements that have been performed, Gaydon and his coworkers concluded from their line-reversal studies⁽¹³⁾ that the actual temperature behind the incident shock wave agreed within about $\pm 30^\circ\text{K}$ with the calculated values for the temperature range from 2000 to 2800°K . The same technique was used by Lapworth⁽³⁰⁾ to get $\pm 50^\circ\text{K}$ agreement behind reflected shocks up to about 2500°K , by Faizullov, et al⁽³¹⁾ with $\pm 100^\circ\text{K}$ agreement up to 5000°K behind incident shocks, and by Charatis⁽³²⁾ with 3% agreement up to 7800°K behind reflected shocks. Wurster and Treanor's results⁽¹⁶⁾ using O_2 ultraviolet absorption behind reflected shocks agreed with the calculated values within about $\pm 100^\circ\text{K}$ from 1500 to 4000°K .

Parkinson and Nicholls' results⁽¹⁴⁾ gave rotational temperatures behind reflected shocks that were about 10 to 15% too low at 6000-9000 $^\circ\text{K}$. This is presently the only discrepancy reported in the literature between calculated and measured shock tube temperatures and is therefore open to question, perhaps on the basis that the thermometric CN molecules in these experiments might have been in a thermal boundary layer near the Mylar membrane clamped in the

shock tube. The temperature range covered by Parkinson and Nicholls is, however, much larger than that covered in other temperature measurements.

Recent calculations by Learner⁽³³⁾ considering vibration-rotation interaction of the OH molecules indicate that measured rotational temperatures, assuming separable electronic and vibrational matrix elements, may be too low by as much as 200°K at 3000°K. Since the spectroscopic temperature measurements of this study are based on intensity ratios of nearly entire vibration-rotation bands, it is expected that the results will not be affected appreciably by vibration-rotation interactions which result mainly in a redistribution of intensities within the bands. These expectations are borne out by the fact that the measured temperatures, assuming constant $|R_{el}|^2$ and $|p_{nn'}|^2$ factors, agree very well with the equilibrium temperature in the 3500°K range.

C. Vibrational Relaxation of OH

The lower trace in Fig. 12 is due to emission primarily from the (2,2)- and (3,3)-vibration-rotation bands in the ${}^2\Sigma \rightarrow {}^2\Pi$ system while the upper trace corresponds to emission primarily from the (0,0)- and (1,1)-bands. Reference to the initial portions of these traces suggests that a time lag is required for the upper vibrational states to come into statistical equilibrium with the lower states.

Approximating the intensity-time relationship for the (2,2)-

and (3,3)-band emission by the expression

$$I = c(t - \tau)(1 - e^{-t/\tau}),$$

it is seen that the vibrational relaxation time (τ) is about $25\mu\text{s}$ for this process. Similar values (15 to $30\mu\text{s}$) were observed in most of the experiments which were performed over a relatively small temperature range. These observed relaxation times are in approximate agreement with the experimental data of Ref. 27 and also with values calculated from the Schwartz-Slowsky-Herzfeld method⁽³⁴⁾ assuming reasonable collision diameters.⁽³⁵⁾

It should be noted that the spectroscopic temperature measurements are not affected by relaxation processes since $\phi(T)$ depends only on the increase of intensity per unit optical depth and is determined from the slopes of the oscilloscope traces.

VII. CONCLUSIONS

The experimental records indicate that isothermal equilibrium is achieved behind the reflected shock wave for the $\text{OH } ^2\Sigma \rightarrow ^2\Pi$ system for a period of time lasting about $200\mu\text{s}$ in the shock tube used for these experiments. The spectroscopic temperatures obtained by monitoring emission from this band system agree well with calculated equilibrium temperatures, thus validating the assumed conditions for the reflected shock region and demonstrating the utility of the wide-band, dual wavelength emission method used in this study.

REFERENCES FOR PART I

1. T. Carrington and N. Davidson, *J. Phys. Chem.* 57, 418 (1953).
2. C.E. Treanor and W.H. Wurster, *J. Chem. Phys.* 32, 758 (1960).
3. J.C. Keck, J.C. Camm and B. Kivel, *J. Chem. Phys.* 28, 723 (1958).
4. M. Lapp, *J. Quant. Spectr. Radiat. Transfer* 1, 30 (1961).
5. T.D. Wilkerson, The Use of the Shock Tube as a Spectroscopic Source with an Application to the Measurement of gf-Value for Lines of Neutral and Singly Ionized Chromium, Ph. D. Thesis and University of Michigan Department of Physics Report No. 02822-3-T, June 1961.
6. H. Mark, The Interaction of a Reflected Shock with the Boundary Layer in a Shock Tube, NACA TM 1418.
7. J.P. Toennies and E.F. Greene, *J. Chem. Phys.* 26, 655 (1957).
8. R.A. Strehlow and A. Cohen, *J. Chem. Phys.* 30, 257 (1959).
9. G.B. Skinner, *J. Chem. Phys.* 31, 268 (1959).
10. T.A. Brabbs, S.A. Zlatarich, F.E. Belles, *J. Chem. Phys.* 33, 307 (1960).
11. R.W. Ditchburn, Sec's 15.18 - 15.29, Light, Interscience Publishers, Inc., New York, 1953.
12. S.S. Penner, pp. 561-574, Fourth Symposium on Temperature, Its Measurement and Control in Science and Industry, Reinhold Publishing Co., New York, 1962.
13. J.G. Clouston, A.G. Gaydon and I.I. Glass, *Proc. Roy. Soc.* 248A, 429 (1958); J.G. Clouston, A.G. Gaydon and I.R. Hurle, *Proc. Roy. Soc.* 252A, 143 (1959); A.G. Gaydon and I.R. Hurle, *Proc. Roy. Soc.* 262A, 38 (1961).
14. W.H. Parkinson and R.W. Nicholls, *Can. J. Phys.* 38, 715 (1960).
15. L. Nadaud and M. Gicquel, Mésure Optique des Températures Elevees, from AGARD meeting on High Temperature Aspects of Hypersonic Flow, Brussels, April, 1962.

16. W.H. Wurster and C.E. Treanor, Spectroscopic Technique for Temperature-Density Measurements in Oxygen-Bearing Flows, Cornell Aeronautical Laboratory Report No. AD-1118-A-10, December 1959.
17. R.A. Allen, J.C. Camm and J.C. Keck, *J. Quant. Spectr. Radiat. Transfer* 1, 269 (1961).
18. R.G. Bennett and F.W. Dalby, *J. Chem. Phys.* 31, 434 (1959).
19. W.H. Wurster, *J. Chem. Phys.* 36, 2111 (1962).
20. G. Charatis and T.D. Wilkerson, *Phys. of Fluids* 2, 578 (1959).
21. S.S. Penner, Quantitative Molecular Spectroscopy and Gas Emissivities, Addison-Wesley Publishing Co., Reading, Mass., 1959.
22. L. Pauling and E.B. Wilson, Chap. X, Introduction to Quantum Mechanics, McGraw-Hill Book Co., Inc., New York, 1935.
23. R.W. Nicholls, *Proc. Phys. Soc., A*, Vol. LXIX, 941 (1956).
24. G.H. Dieke and H.M. Crosswhite, *J. Quant. Spectr. Radiat. Transfer*, 2, 97 (1962).
25. K.E. Schuler, *J. Chem. Phys.* 18, 1221 (1950).
26. T.A. Jacobs, Consideration of Some Electronic Components in Shock Tube Instrumentation, Guggenheim Jet Propulsion Center TR No. 2, Contract AF 49(638)-984, California Institute of Technology, February, 1961.
27. S.H. Bauer, G.L. Schott and R.E. Duff, *J. Chem. Phys.* 28, 1089 (1958).
28. S.S. Penner, Chap. XIX, Chemistry Problems in Jet Propulsion, Pergamon Press, New York, 1957.
29. R.F. Barrow, *Arkiv Fysik*, 11, 281 (1956); *Proc. Phys. Soc. (London)*, A69, 178 (1956). Also private communication with H.W. Wooley, National Bureau of Standards.
30. K.C. Lapworth, Temperature Measurements in a Hypersonic Shock Tunnel, from AGARD meeting on High Temperature Aspects of Hypersonic Flow, Brussels, April, 1962.

31. F. S. Faizullof, N. N. Sovolev, and E. M. Kudryavtsev, Optika i Spektrosk. 8, 761 (1960b); see Opt. Soc. Amer. Translations 8, 400.
32. G. Charatis, Shock Tube Determination of Chromium gf-Values, Ph. D. Thesis, University of Michigan (1962).
33. R. C. M. Learner, Proc. Roy. Soc. 269A, 311 (1962).
34. R. N. Schwartz, Z. I. Slawsky, and K. F. Kerzfeld, J. Chem. Phys. 20, 1591 (1952).
35. K. F. Herzfeld and T. A. Litovitz, p. 328, Absorption and Dispersion of Ultrasonic Waves, Academic Press, New York (1959).

PART II. SHOCK TUBE MEASUREMENTS OF THE ABSORPTION
OSCILLATOR STRENGTH FOR THE ${}^2\Sigma \rightarrow {}^2\Pi$
ELECTRONIC BAND SYSTEM OF OH

I. INTRODUCTION

The absolute value of oscillator strengths,⁽⁵⁾ or the equivalent transition probabilities of atoms and molecules, are of interest for a number of reasons, including their use in the calculation of radiant heat transfer to hypersonic vehicles,⁽⁶⁾ stellar atmosphere studies,⁽⁷⁾ optical determination of population temperatures,⁽⁸⁾ etc.

Only for the simplest atomic systems can the f-numbers be calculated with reasonable confidence.⁽⁹⁾ The theoretical problem is, of course, much more complicated for molecules, and there are only a relatively few molecular systems for which experimental f-number measurements are available.

There are three principal types of experiments that have been used to obtain absolute f-numbers for molecules. These are: (a) measurements of lifetime-decays of high-energy states excited by electron gun bombardment;^(10, 11) (b) measurements of integrated absorption spectra;^(2-4, 12) (c) measurements based on absolute intensity calibrations of emission spectra.^(1, 13, 14)

The lifetime measurements of Bennett and Dalby^(10, 11) illustrate the most elegant of these three methods. An electron gun was pulsed so as to irradiate molecules for durations of about four

times their radiative lifetime. The lifetime was measured from records of the free decay of light emission associated with the molecular band. A clever pulsing system was used, with the photomultiplier detector being turned on at slightly different times throughout a series of cycles. The resulting output signal was integrated and displayed on a chart recorder. The molecular lifetimes were obtained from semi-logarithmic plots using these records and were then related to the electronic f-number by the following theoretical formula (see, for example, Chap. 2, Ref. 15):

$$(f_{\ell \rightarrow u})_{el} = \frac{m_e c \lambda^2}{8\pi^2 e^2} \frac{g_u}{g_\ell} \frac{1}{\tau}$$

where $(f_{\ell \rightarrow u})_e$ is the absorption oscillator strength for the band system, m_e is the electron mass, e the electron charge, c the velocity of light, λ the average wavelength for the system (e.g., the band head), g_u and g_ℓ the degeneracies for the upper and lower electronic states, and τ is the decay time of the light emission. The lifetime-decay experiments are inherently very "clean", the only source of possible systematic error being that cascading from higher states may feed the population in the lower radiating state, thus leading to longer apparent lifetimes and hence low f-numbers.

The absorption measurements^(2-4,12) are usually performed by observing a light source through a cell containing a known concentration of absorbing molecules. For a low concentration, i.e.,

the transparent gas case, the integrated absorption of individual spectral lines is given by⁽²⁾

$$NfL = \frac{m_e c^2}{\pi e} \int P' X d\omega$$

where N is the number of absorbing molecules per unit volume, f is the f-number for the particular line observed, L the effective path length, P' the absorption coefficient per molecule, X the optical depth of the absorbing molecules, and the integration extends over the line profile. If the transparent approximation is not valid, the experimental data may be fitted to appropriate curves of growth^(2,4,15) and f-numbers determined from these.

The main difficulty in the absorption experiments is associated with the requirement of high resolution spectrography. Flame measurements may have large errors from temperature gradients and concentration non-uniformities.

Although some absolute measurements have been performed on the emission of atoms in stellar atmospheres and flames (see, for example, Ref. 16), none appear to have been made on molecules under these conditions because the required excitation energies for strong intensities are relatively high. The very high temperatures and relatively uniform properties available in shock tubes have popularized this instrument as a spectroscopic light source for molecular and atomic f-number experiments^(1,12-15,17) in recent years (since ~ 1952).

The technique usually involves monitoring the emission in fairly wide spectral regions covering the system of interest, and then relating the relative response of the detection system to an absolute level by employing the output of a standard lamp.

The ease of attaining high temperatures in shock tubes simplifies the task of exciting the required spectra, but the problems of impurity radiation, attainment of equilibrium, and the absolute intensity calibration, combined with the usual spectrometric instrumental problems, can result in large discrepancies in f-numbers reported for the same molecular system (see, for example, Refs. 13, 14, and 18). Hence, despite its apparent advantages, use of the high-enthalpy shock tube entails important experimental difficulties. However, it is to be expected that agreement between measurements will ultimately be satisfactory once the numerous sources of systematic error have been eliminated. A study of the more subtle errors, and the development of techniques for eliminating these errors, constitute the principal contributions made in the present investigations.

The history of OH f-number measurements in this Laboratory dates back to 1953 when Dyne⁽⁴⁾ performed absorption measurements on OH as a check on Oldenberg and Rieke's original experiments,⁽³⁾ (which were made in 1938). Dyne's measurement was undertaken since the f-value for OH is often used in connection with rotational population temperatures in flames,⁽¹⁹⁾ Because Dyne's measurements were not entirely satisfactory and because his result

for the f-number was about one-half that of Oldenberg and Rieke, a shock tube experiment on OH was initiated in this Laboratory in 1958 by Lapp⁽¹⁾ and completed in 1960. An OH absorption measurement in a flame was reported by Carrington⁽²⁾ in 1959.

Although Lapp's f-number was in accord with that of Oldenberg and Rieke, a check of the apparatus used for the shock tube experiment uncovered an error in the absolute intensity calibration associated with internal light scattering in the monochromator. In addition, some questions arose concerning the determination of the initial mixture concentration in the shock tube (see Part I of this thesis and also Section III of this part for further discussion of these points). For these reasons, a second series of shock tube experiments was performed to remeasure the OH f-number, and these experiments form the basis for the study reported here. Concurrent with the f-number measurements, a spectroscopic technique for measuring the temperature of the OH species was devised to check the validity of the assumed equilibrium shock tube temperatures calculated from one-dimensional flow theory. The results of the spectroscopic temperatures confirmed the calculated values and are described in Part I of this thesis.

The apparatus for the OH f-number measurement and the spectroscopic temperature experiment was basically the same, except that a dual monochromator arrangement was used in the temperature measurement to monitor radiation from two regions of the

$\text{OH}^2 \sum \rightarrow^2 \Pi$ system. Some of the discussion in the following sections parallels that of Part I, but the emphasis in Part II is placed on the absolute intensity calibration. Some of the details of the experimental equipment given in Part I are omitted in the present discussion.

II. THEORETICAL CONSIDERATIONS

In this section, the relationship between the relative emission from the shock-tube experiment and the absolute flux from a standard light source is established. The requirements of the shock tube and calibration optics are examined and the electronic f-number for the band system is expressed in terms of the measured variables of the shock tube experiment and the associated calibration.

A. The Shock Tube Experiment

The shock tube optical system receives light flux emitted from a window viewing axial radiation from the shock tube, as shown in Fig. 1. The optical system is focused on the exit window since this is the source of the light emission to be studied.

The spectral light flux (per unit wavenumber interval) subtended by the exit optics is given by

$$\mathcal{F}_{\omega, g} = \pi \epsilon_{\omega, g} B_{\omega, g}^0 (\sin^2 \alpha) A_e \quad (1)$$

where ϵ_{ω} is the spectral emissivity of the gas, B_{ω}^0 is the blackbody spectral steradiancy (or luminance), α is the half-angle subtended by the exit optics, A_e is the effective area of the exit window as

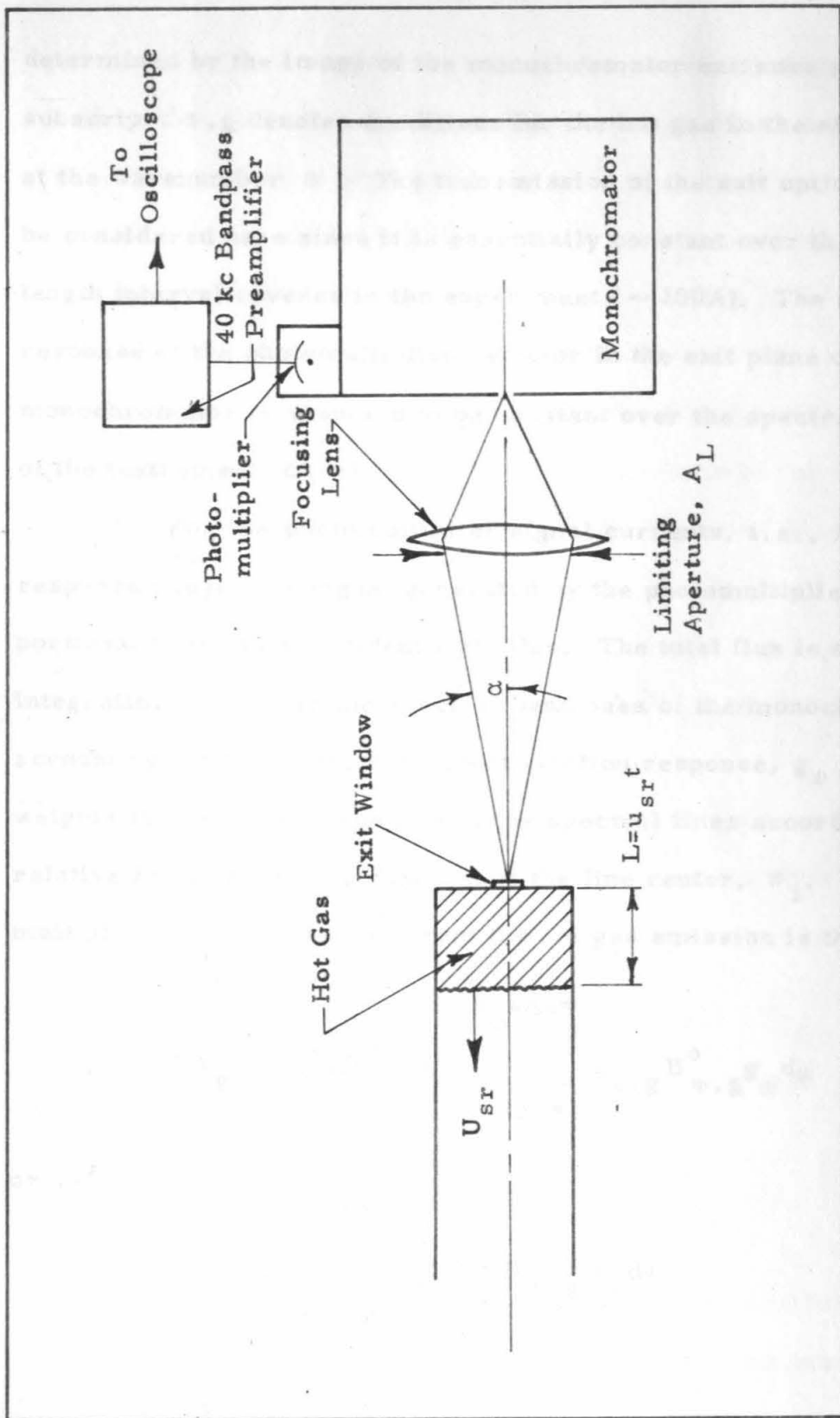


Fig. 1. Schematic diagram of the shock tube exit optics.

determined by the image of the monochromator entrance slit, and the subscript ω, g denotes conditions for the hot gas in the shock tube at the wavenumber ω . The transmission of the exit optics need not be considered here since it is essentially constant over the wavelength interval covered in the experiment ($\sim 100\text{\AA}$). The spectral response of the photomultiplier detector in the exit plane of the monochromator is assumed to be constant over the spectral band pass of the instrument ($2\Delta\omega^*$).

For low photomultiplier signal currents, i. e., in the linear response range, the signal generated by the photomultiplier is proportional to the total incident light flux. The total flux is obtained by integrating Eq. 1 over the spectral band pass of the monochromator accounting for the instrumental slit function response, g_{ω} , which weights the relative intensities of the spectral lines according to the relative height of the slit function at the line center, ω_i . The photomultiplier voltage resulting from the hot gas emission is thus given by

$$V_g = K' \pi (\sin^2 \alpha) A_e \int_{\omega_o - \Delta\omega^*}^{\omega_o + \Delta\omega^*} \epsilon_{\omega, g} B_{\omega, g}^o g_{\omega} d\omega$$

or

$$V_g = K \int_{\omega_o - \Delta\omega^*}^{\omega_o + \Delta\omega^*} \epsilon_{\omega, g} B_{\omega, g}^o g_{\omega} d\omega \quad (2)$$

where ω_0 is the wavenumber setting of the monochromator and K is the absolute sensitivity of the optical-detection system expressed as signal voltage/watt of light input per cm^2 per steradian. For a particular experimental configuration, K is a constant and is determined by the standard lamp calibration.

In terms of the spectral absorption coefficient, P_{ω} , for each of the lines within the slit function base and the optical depth, X (which is the product of p_{OH} , the partial pressure of the emitting species, and L, the geometrical path length of emission), Eq. 2 becomes

$$V_g = K \left[\sum_i \int_{\omega_0 - \Delta\omega^*}^{\omega_0 + \Delta\omega^*} [1 - \exp(-P_{\omega_i} X)] B_{\omega, g}^{\circ} g_{\omega} d\omega \right]_{2\Delta\omega^*} \quad (3)$$

where the summation extends over all the i spectral lines within $2\Delta\omega^*$. For an optically thin gas, $P_{\omega_i} X \ll 1$, and since the widths of individual spectral lines are small compared to $2\Delta\omega^*$, Eq. 3 may be written as

$$V_g = KX \left[\sum_i B_{\omega_i}^{\circ} g_{\omega_i} \int_{\text{line}} P_{\omega_i} d\omega \right]_{2\Delta\omega^*}$$

or

$$V_g = KX \left[\sum_i B_{\omega_i}^{\circ} g_{\omega_i} S_{\omega_i} \right]_{2\Delta\omega^*} \quad (4)$$

where S_{ω_i} is the integrated intensity for the ith spectral line at ω_i .

Because of the slit function, g_{ω} , it is seen that V_g

represents only some fraction of the total emission intensity from the wavelength region monitored [primarily the (0,0)-band], and this fraction of the total band emission must be determined.

If the monochromator had a flat response over the whole band, i. e., if $g_{\omega} = 1.0$ everywhere, the equivalent expression for the theoretical signal voltage from the (0,0)-band would be

$$V_{g(0,0)} = KX \left[\sum_i B_{\omega_i}^o S_{\omega_i} \right]_{(0,0)} \quad (5)$$

and the fraction of the (0,0)-band emission passed by the monochromator would be $V_g/V_{g(0,0)} = G(T)$. The values of the S_{ω_i} terms in Eqs. 4 and 5 may be expressed in terms of the electronic, vibrational, and rotational matrix element terms, as shown in Part I, so that

$$\left[\sum_i B_{\omega_i}^o g_{\omega_i} S_{\omega_i} \right]_{2\Delta\omega^*} = \frac{16\pi^3 c}{3kTQ} |R_{el}|^2 \left[\sum_{nn'} |p_{nn'}|^2 \sum_b \sum_i \omega_i^4 \exp(-E_{u_i}/kT) |p_{kk'}|_i^2 g_{\omega_i} \right]_{2\Delta\omega^*} \quad (6)$$

and similarly,

$$\left[\sum_i B_{\omega_i}^o S_{\omega_i} \right]_{(0,0)} = \frac{16\pi^3 c}{3kTQ} |R_{el}|^2 |p_{0,0}|^2 \left[\sum_b \sum_i \omega_i^4 \exp(-E_{u_i}/kT) |p_{kk'}|_i^2 \right]_{(0,0)} \quad (7)$$

Here $|R_{e\ell}|^2$ is the square of the electronic matrix element, $|p_{nn'}|^2$ the square of the vibrational matrix element for the (n, n') -band, $|p_{kk'}|_i^2$ the square of the rotational matrix element for the i th spectral line, Q the internal partition function, E_{u_i} the energy level for the upper state of the i th line, and the summations extend over all the i lines in all branches and in the case of Eq. 6 over all the bands which are encompassed by the slit function, $2\Delta\omega^*$. The fraction of the total emission of the $(0, 0)$ -band that is passed by the monochromator is then given by the ratio of Eqs. 6 and 7, viz.,

$$\frac{\left[\sum_i B_{\omega_i}^o g_{\omega_i} S_{\omega_i} \right]_{2\Delta\omega^*}}{\left[\sum_i B_{\omega_i}^o S_{\omega_i} \right]_{(0,0)}} = G(T) \quad (8)$$

where $G(T)$ may be obtained conveniently by using a computing machine routine for the expression

$$G(T) = \frac{\left[\sum_{nn'} |p_{nn'}|^2 \sum_b \sum_i \omega_i^4 \exp(-E_{u_i}/kT) |p_{kk'}|_i^2 g_{\omega_i} \right]_{2\Delta\omega^*}}{|p_{0,0}|^2 \left[\sum_b \sum_i \omega_i^4 \exp(-E_{u_i}/kT) |p_{kk'}|_i^2 \right]_{(0,0)}} \quad (9)$$

Calculations for Eq. 9 were performed on an IBM 7090 using the relative rotational transition probabilities, line locations, and energy levels of Dieke and Crosswhite.⁽²⁰⁾ The triangular slit function of

Fig. 2 and Nicholl's⁽²¹⁾ vibrational overlap integral data were used. The results for a slit width of 100A at 3090A near the $^2\Sigma \rightarrow ^2\Pi$ band head are shown in Fig. 3. Most of the intensity contribution to the signal is from the (0,0)-band with the (1,1)-band contributing about $2\frac{1}{2}\%$ around 3500^oK. The decrease in G(T) with increasing temperature is due to the shift in population to higher bands as the gas gets hotter.

The total integrated intensity $\alpha(0,0)$ for the (0,0)-band is related to the theoretical signal voltage for the entire (0,0)-band by the expression

$$V_{g(0,0)} = KXB_{\omega_{o,g}}^o \int_{(0,0)} P_{\omega} d\omega$$

or

$$V_{g(0,0)} = KXB_{\omega_{o,g}}^o \alpha(0,0) \quad (10)$$

where $B_{\omega_{o,g}}^o$ is the blackbody spectral steradiance at an average wavenumber for the band (e.g., near the band head, $\bar{\omega}_{0,0}$). Combining Eqs. 4, 5, 8 and 10 then yields the result

$$\alpha(0,0) = \frac{V_g}{G(T)KX B_{\omega_{o,g}}^o} \quad (11)$$

This total integrated intensity for the (0,0)-band is related to the vibrational f-number for the (0,0)-band through the expression

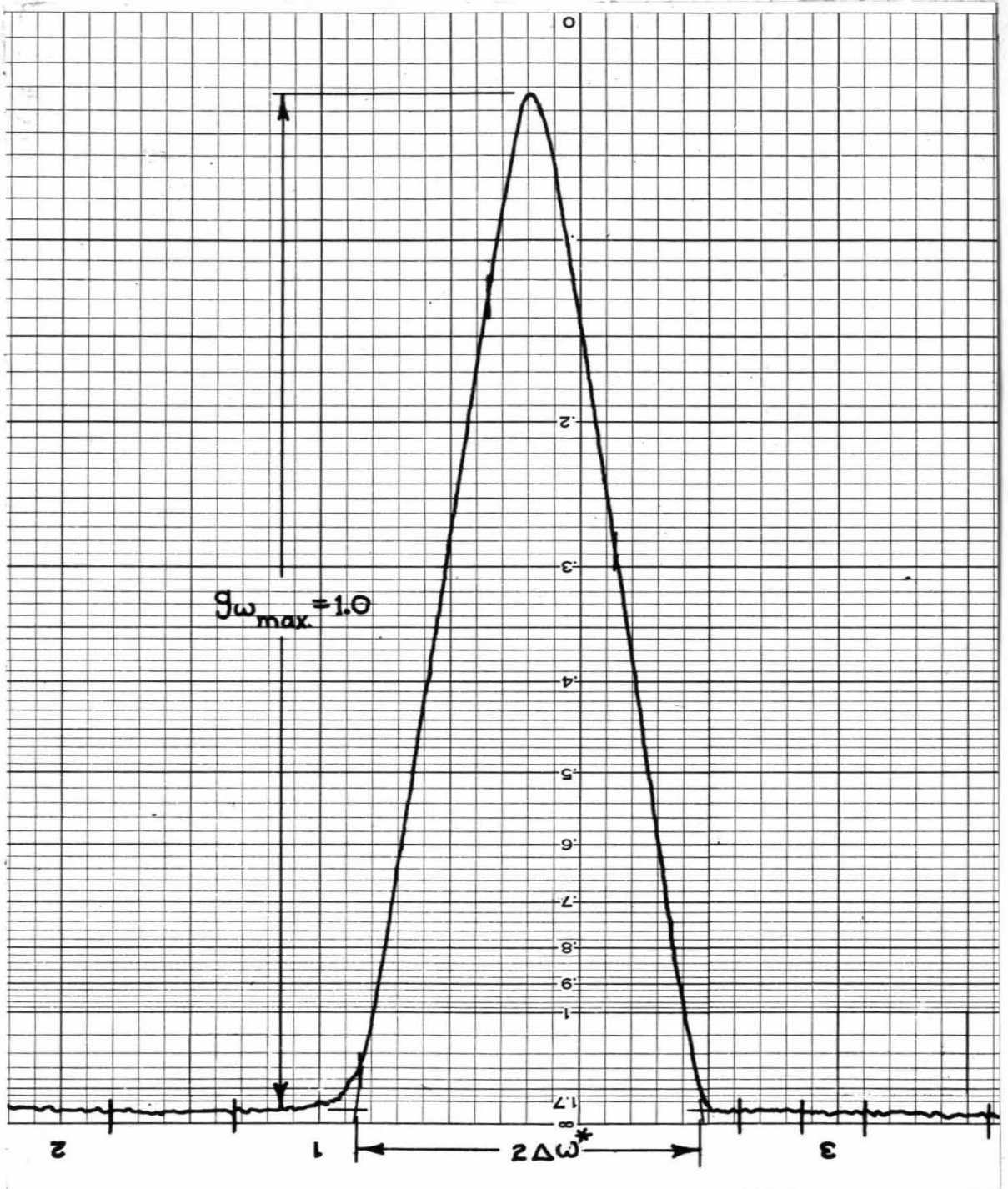


Fig. 2. The monochromator slit function as determined by scanning the 3341.48 Hg line with a thermocouple; the monochromator slit width setting is 1.0 mm.

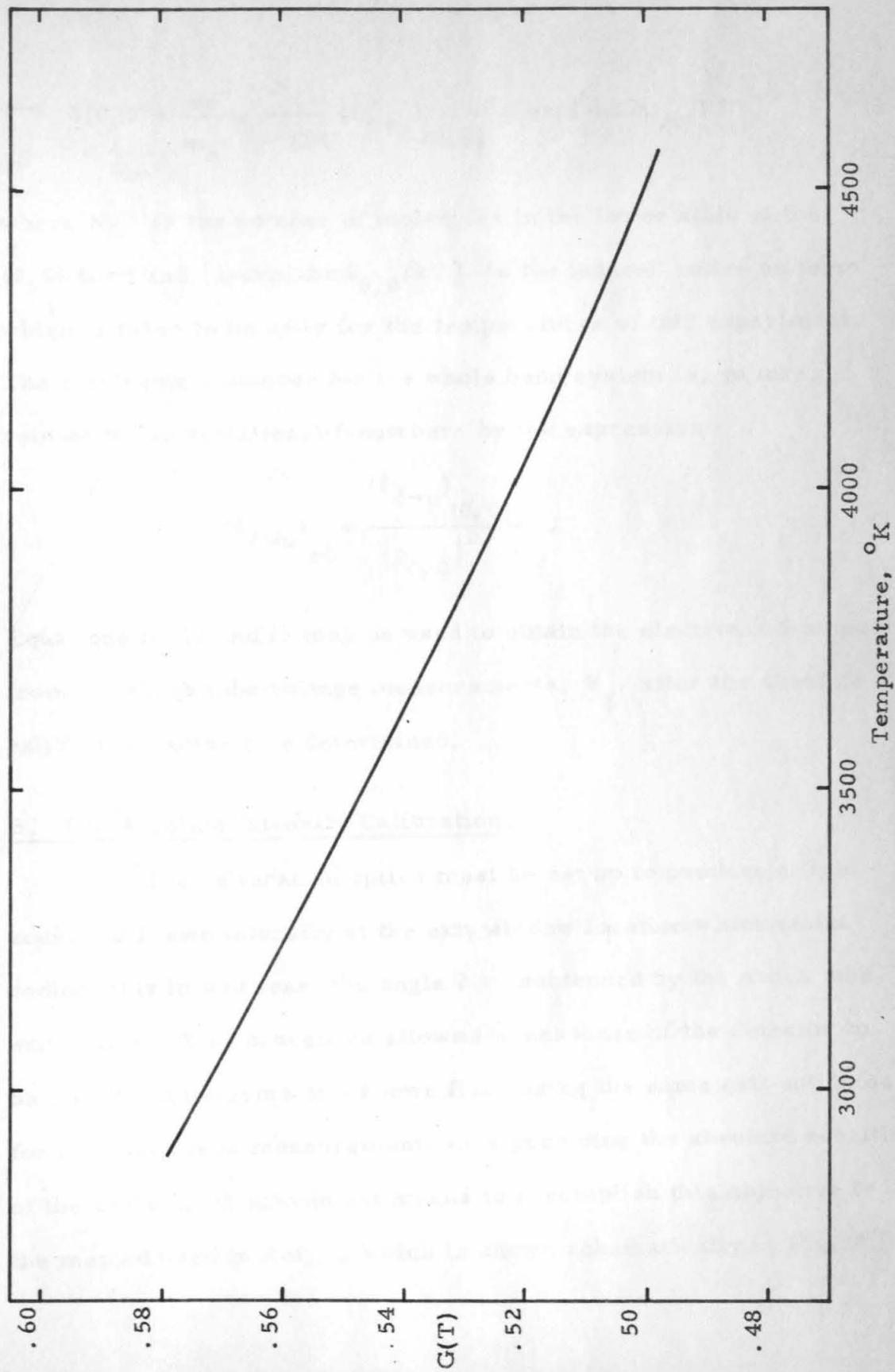


Fig. 3. $G(T)$, the calculated fraction of the $(0, 0)$ -band intensity passed by a triangular slit function with $\omega_0 = 3090\text{A}$ and $2\Delta\omega = 100\text{A}$.

$$\alpha(0,0) = \frac{\pi e^2}{m_e c^2} \frac{N_\ell}{P_{OH}} (f_{\ell \rightarrow u})_{(0,0)} [1 - \exp(-hc \bar{\omega}_{0,0}/kT)] \quad (12)$$

where N_ℓ is the number of molecules in the lower state of the (0,0)-band and $[1 - \exp(-hc \bar{\omega}_{0,0}/kT)]$ is the induced emission term which is taken to be unity for the temperatures of this experiment. The electronic f-number for the whole band system is, in turn, related to the vibrational f-number by the expression

$$(f_{\ell \rightarrow u})_{el} = \frac{(f_{\ell \rightarrow u})_{(0,0)}}{|p_{0,0}|^2} \quad (13)$$

Equations 11, 12 and 13 may be used to obtain the electronic f-number from the shock tube voltage measurements, V_g , after the absolute calibration factor K is determined.

B. The Absolute Intensity Calibration.

The calibration optics must be set up to produce a light source of known intensity at the exit window location which emits radiant flux into at least the angle 2α subtended by the shock tube exit optics. This procedure allows the response of the detector to be measured in terms of a known flux, using the same exit optics as for the shock tube measurement, thus providing the absolute sensitivity of the system. A convenient means to accomplish this objective is the method used in Ref. 1, which is shown schematically in Fig. 4.

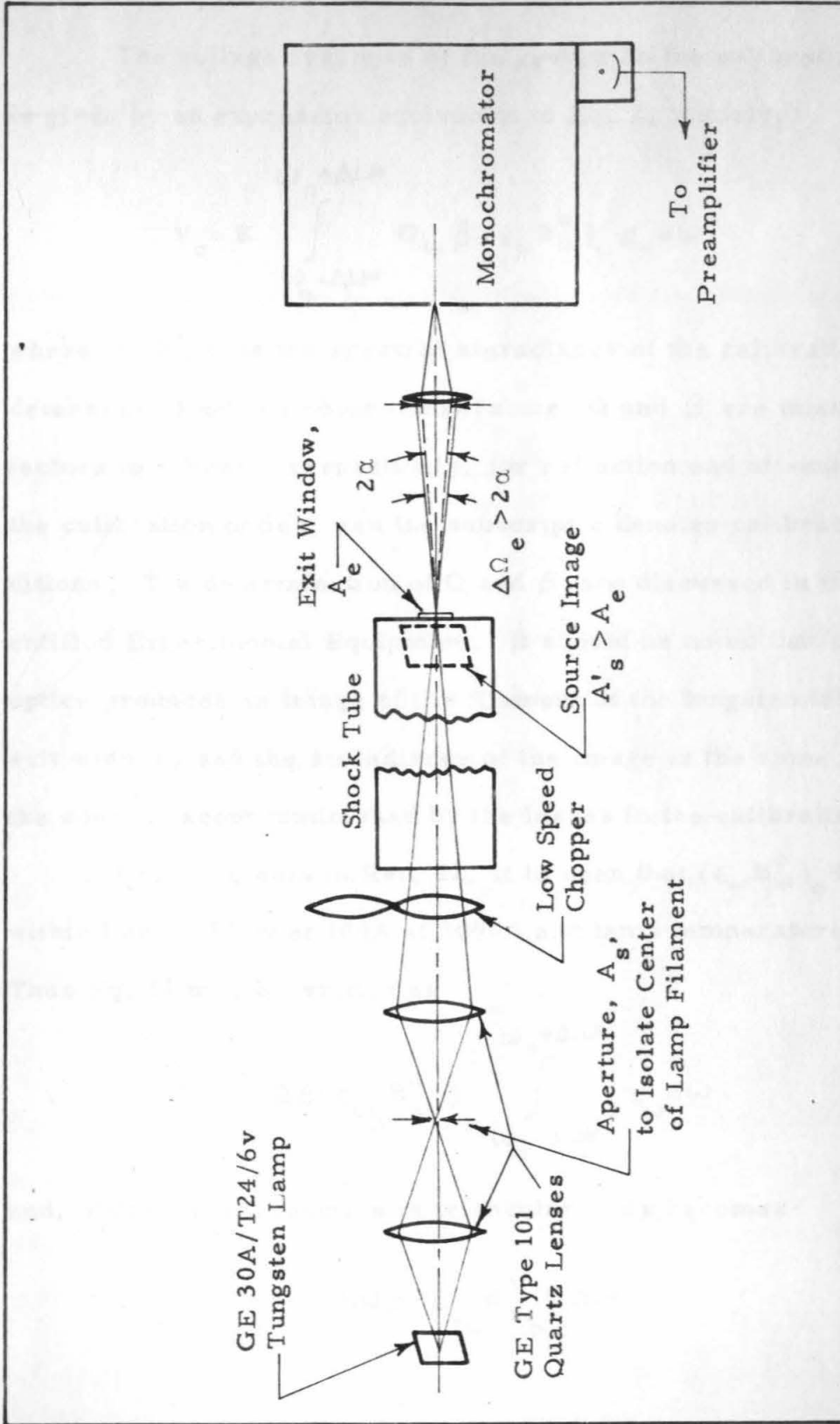


Fig. 4. Schematic diagram of the absolute intensity calibration optics.

The voltage response of the system to the calibration light is given by an expression equivalent to Eq. 2, namely,

$$V_c = K \int_{\omega_o - \Delta\omega^*}^{\omega_o + \Delta\omega^*} Q_\omega \beta (\epsilon_\omega B_\omega^o)_c g_\omega d\omega \quad (14)$$

where $(\epsilon_\omega B_\omega^o)_c$ is the spectral steradiance of the calibration lamp as determined from its color temperature, Q and β are intensity loss factors to account, respectively, for reflection and off-axis losses in the calibration optics, and the subscript c denotes calibration conditions. The determination of Q and β are discussed in the section entitled Experimental Equipment. It should be noted that the calibration optics produces an image of the filament of the tungsten lamp on the exit window, and the steradiance of the image is the same as that of the source except diminished by the losses in the calibration optics.

From the data in Ref. 22, it is seen that $(\epsilon_\omega B_\omega^o)_c$ is constant within 1 and 1/2% over 100A at 3090A and lamp temperatures of 2500°K. Thus Eq. 14 may be written as

$$V_c = KQ\beta (\epsilon_{\omega_o} B_{\omega_o}^o)_c \int_{\omega_o - \Delta\omega^*}^{\omega_o + \Delta\omega^*} g_\omega d\omega$$

and, since the slit function is triangular, this becomes

$$V_c = KQ\beta (\epsilon_{\omega_o} B_{\omega_o}^o)_c \Delta\omega^* . \quad (15)$$

Thus the absolute sensitivity of the exit optics and detector system is given by

$$K = \frac{V_c}{Q\beta (\epsilon_{\omega_o} B_{\omega_o c}^o) \Delta\omega^*} \quad (16)$$

Combining Eqs. 11, 12, 13 and 16, the electronic f-number for the OH system may be written as

$$(f_{\ell \rightarrow u})_{el} = \frac{V_g Q\beta (\epsilon_{\omega_o} B_{\omega_o c}^o) \Delta\omega^* kT_g}{GV_c p_{OH} (u_{sr} t) B_{\omega_{o,g}}^o (\pi e^2 / m_e c^2) [1 - \exp(-hc\omega_{vib}/kT)] |p_{0,0}|^2} \quad (17)$$

where T_g is the gas temperature behind the reflected shock, p_{OH} is the partial pressure of the OH, $u_{sr} t = L$ is the length of hot test gas observed, and ω_{vib} is the vibrational constant for OH (3735.21 cm^{-1}). (20)

Here the approximation has been made that (23)

$$(N_{\ell})_{(0,0)} = \frac{N_{OH}}{Q'_{vib}} = N_{OH} [1 - \exp(-hc\omega_{vib}/kT)]$$

and the ideal gas law

$$N_{OH} = \frac{p_{OH}}{kT_g}$$

has been used. The angle, 2α , of the exit optics is less than $\tan^{-1}(.04)$, so that the optical system "sees" only a one-dimensional cylinder in the core of the hot gas region, and the optical depth is taken as

$$X = p_{OH} u_{sr} t.$$

Equation 17 is an explicit relation for the electronic f-number in terms of the measured variables and was used to obtain the value reported in the present study.

III. EXPERIMENTAL EQUIPMENT

The shock tube and associated equipment were the same as described in Part I. A flushing procedure was used to allow the test gas mixture of water vapor and argon to flow continuously through the shock tube, for periods of about one-half hour before each experiment, to insure that the concentration was uniform and at saturated vapor conditions.⁽²⁴⁾ This procedure allowed the metal shock tube walls and gas-handling system to reach adsorption equilibrium before the flushing was terminated.

An overall view of the apparatus is shown in Fig. 5.

A. Shock Tube Exit Optics

The optical system located at the end of the shock tube is shown schematically in Fig. 1. A Perkin-Elmer model 98 monochromator with a fused silica prism was used to isolate the desired spectral interval extending from 3040 to 3140Å and including the 3064Å band head of the $\sum^2 \rightarrow \Pi^2$ system. A schematic view of the monochromator optics is shown in Fig. 6. Viewing emission axially behind the reflected shock allows an experimental check to be made on the assumptions that the gas is transparent and in equilibrium. Determinations of the slit function and wavelength calibration are discussed in Part I.



Fig. 5. Overall view of the experimental equipment.

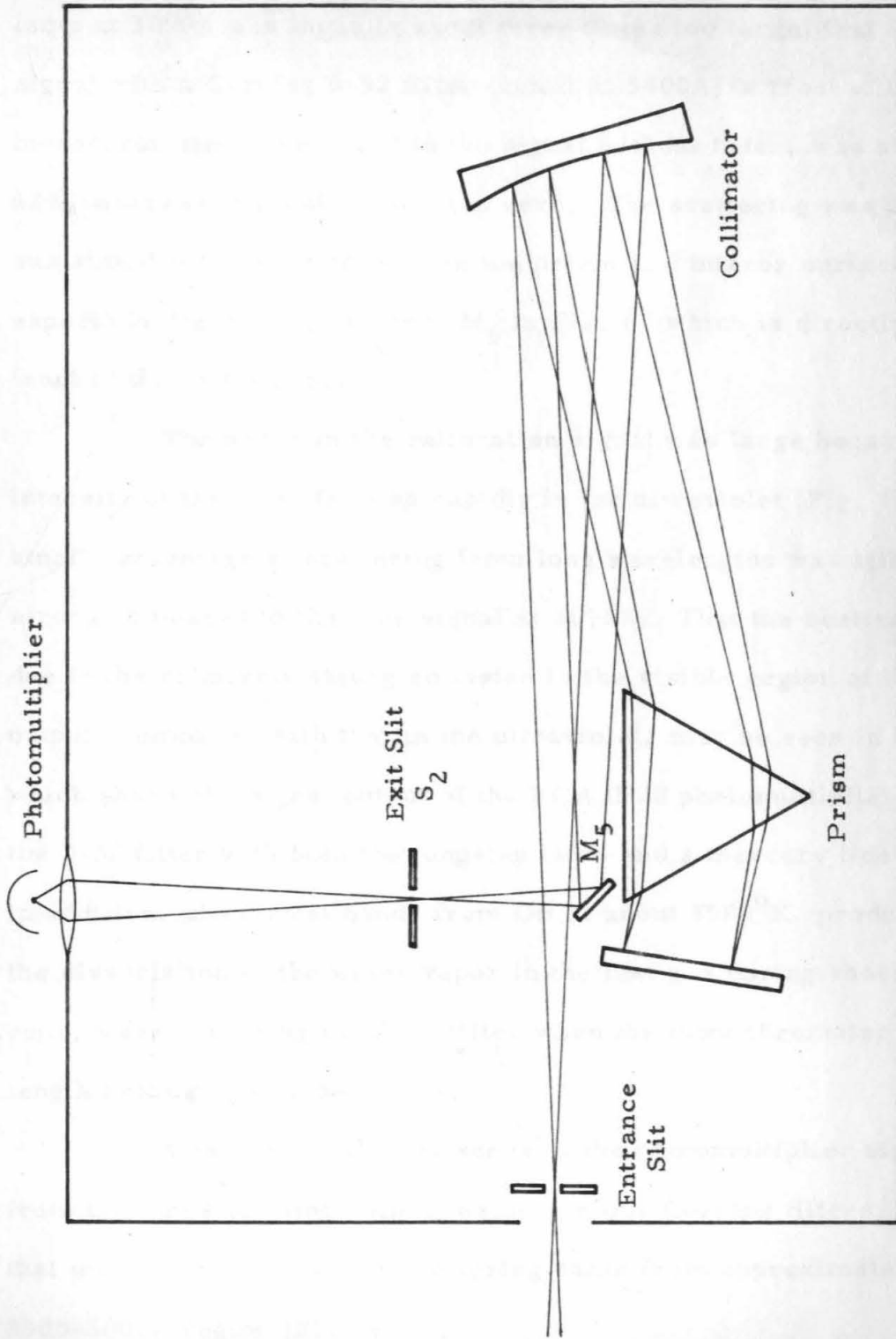


Fig. 6. Schematic view of the internal optics of the monochromator.

It was found that the absolute calibration signal from the lamp at 3090A was initially about three times too large; that is, the signal with a Corning 0-52 filter (cutoff at 3400A) in front of the monochromator, compared to the signal without filter, was about 62%, whereas it should have been zero. The scattering was presumably due to reflections from the prism and mirror surfaces, especially the diagonal mirror M_5 in Fig. 6, which is directly in front of the exit slit S_2 .

The error in the calibration signal was large because the intensity of the lamp falls so rapidly in the ultraviolet (Fig. 7) that a small percentage of scattering from long wavelengths was still strong compared to the true signal at 3090A. That the scattering was due to the relatively strong emission in the visible region of the lamp output, compared with that in the ultraviolet, may be seen in Fig. 8, which shows the signal output of the RCA 1P28 photomultiplier using the 0-52 filter with both the tungsten lamp and a mercury line source. In addition, ultraviolet bands from OH at about 3500^oK, produced by the dissociation of the water vapor in the test gas during shock tube runs, were cut off by the 0-52 filter when the monochromator wavelength setting was below 3400A.

A series of spectral scans of the photomultiplier signal from the tungsten lamp output, using various Corning filters, showed that most of the ultraviolet scattering came from approximately the 3500-5000A region (Fig. 9).

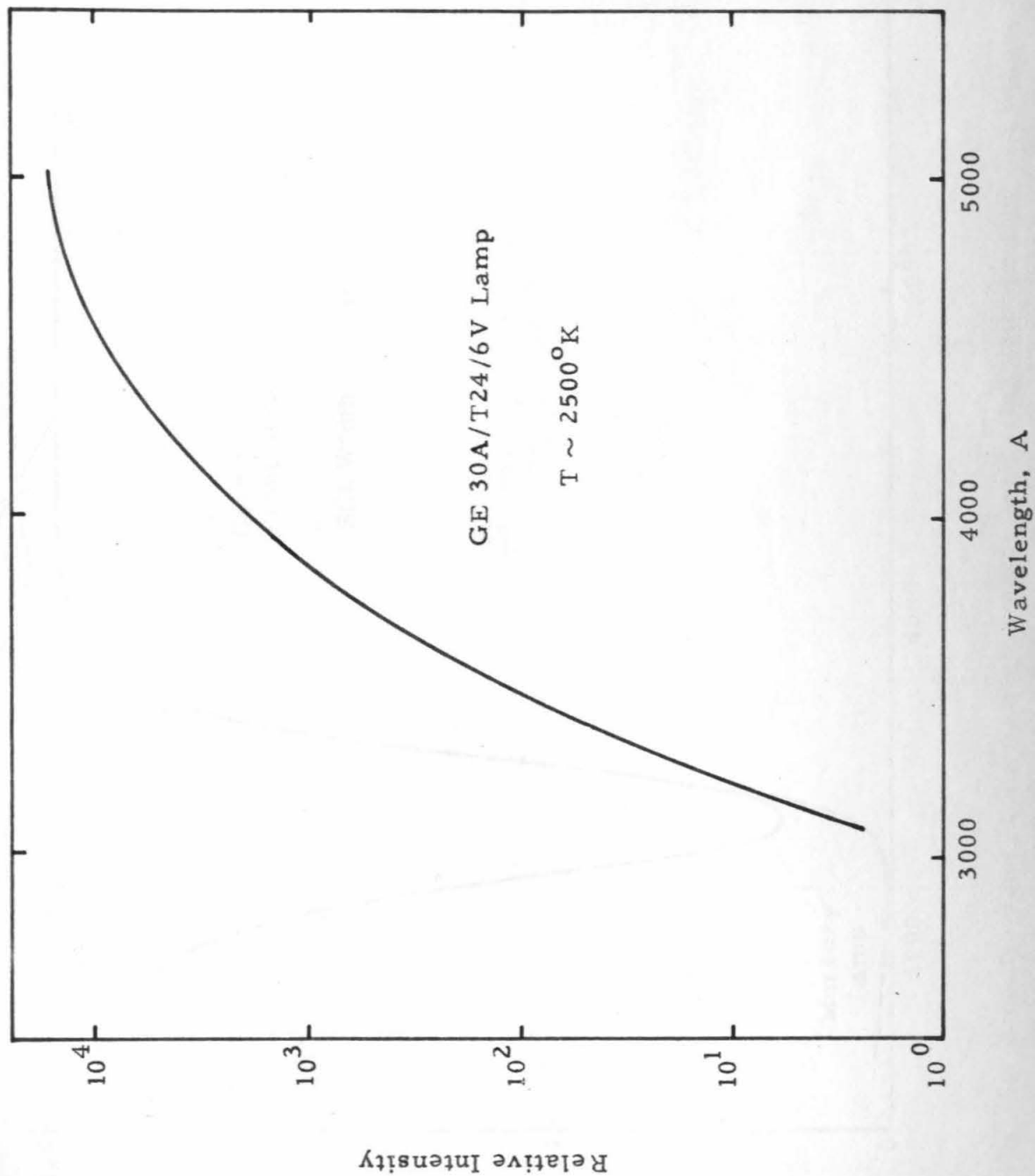


Fig. 7. Relative intensity vs. wavelength for the tungsten calibration lamp.

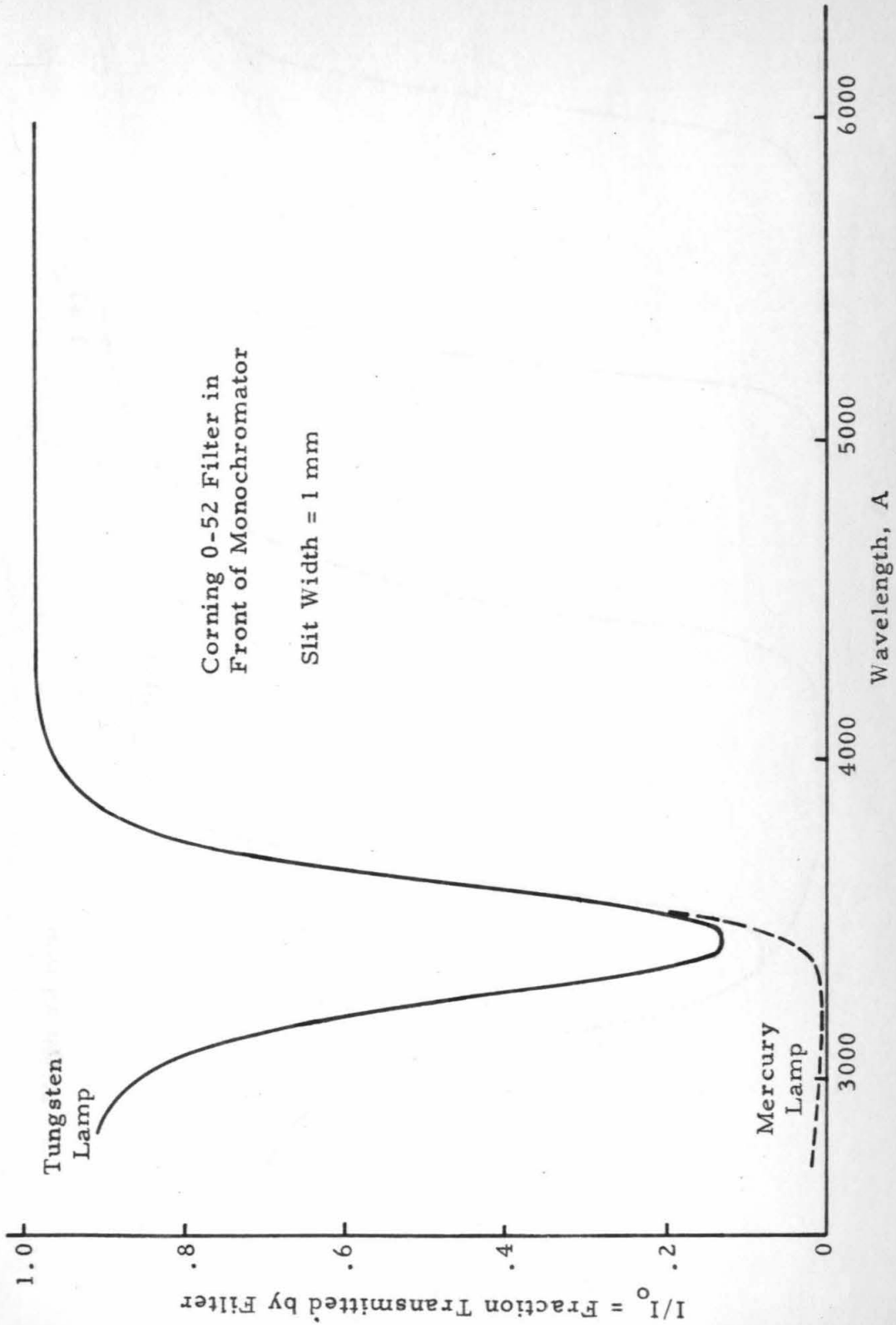


Fig. 8. A comparison of the monochromator scattering with the tungsten calibration lamp and a low-pressure Hg line source.

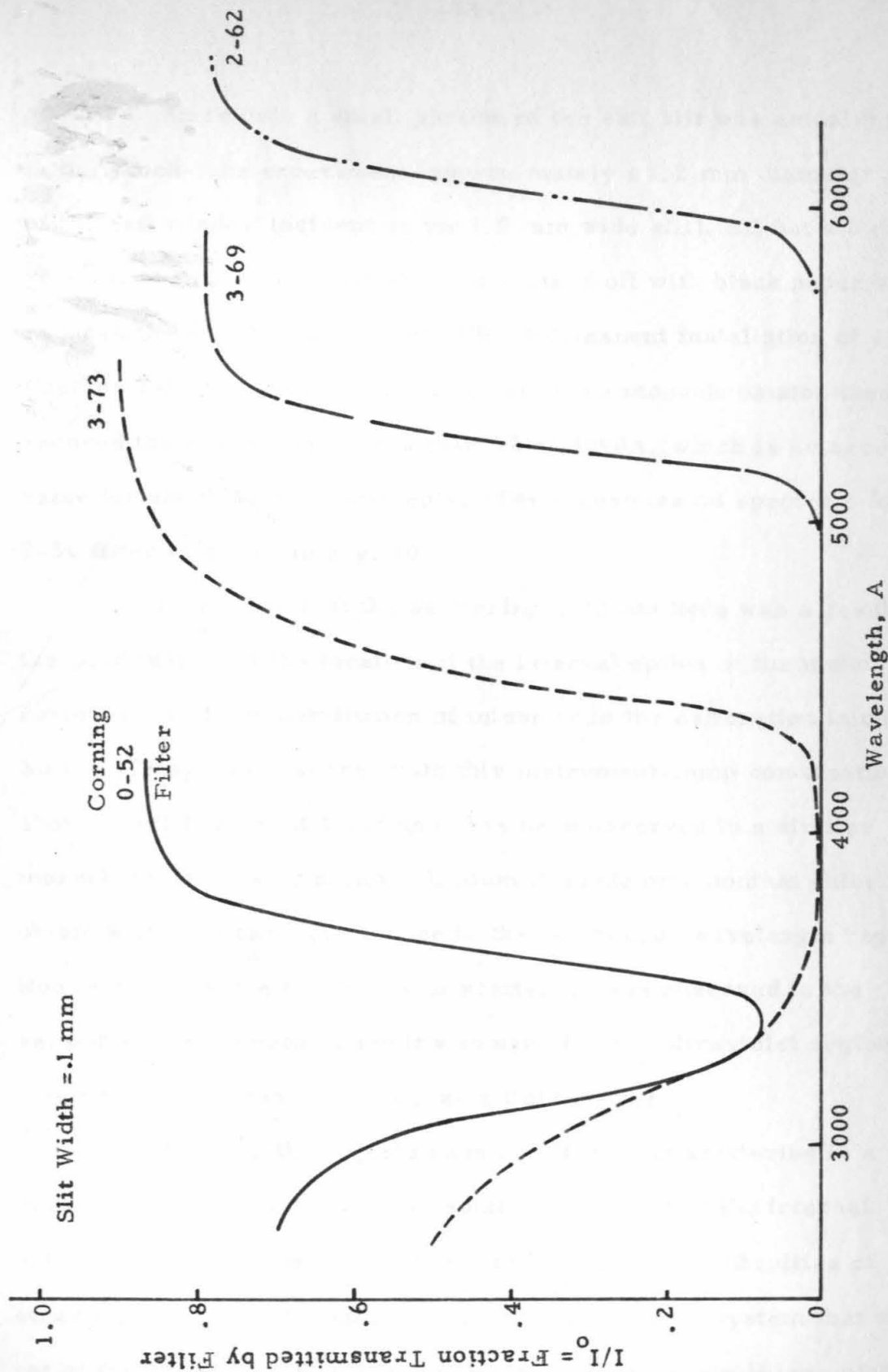


Fig. 9. The effect of various filters on the monochromator scattering with the tungsten calibration lamp.

Since only a small portion of the exit slit was actually used in the shock-tube experiment (approximately a 1.2 mm diameter image of the exit window incident on the 1.0 mm wide slit), all but a 2 mm vertical section of the exit slit was masked off with black paper which reduced the scattering to about 40%. Permanent installation of a Corning 7-54 ultraviolet filter in front of the monochromator then reduced the scattering to less than 5% at 3090A, which is an acceptable value for shock tube experiments. The transmission spectrum for the 7-54 filter is shown in Fig. 10.

It is clear that the scattering problem here was a result of the combination of the location of the internal optics of the monochromator and the distribution of intensity in the calibration lamp. No scattering was observed with this instrument-lamp combination above about 3600-3800A and none has been observed in a similar monochromator using either a lithium fluoride or a sodium chloride prism with a globar light source in the 1-5 micron wavelength region. However, the same magnitude of scattering was observed in the second monochromator when it was used for the ultraviolet region together with the tungsten lamp as a light source.

Although the objects causing ultraviolet scattering in a monochromator are difficult to isolate, the layout of the internal optics for a Littrow mounting tends to increase the difficulties of stray light. An equivalent monochromator-detector system that was not of the Littrow type, for example, a medium quartz Hilger with a

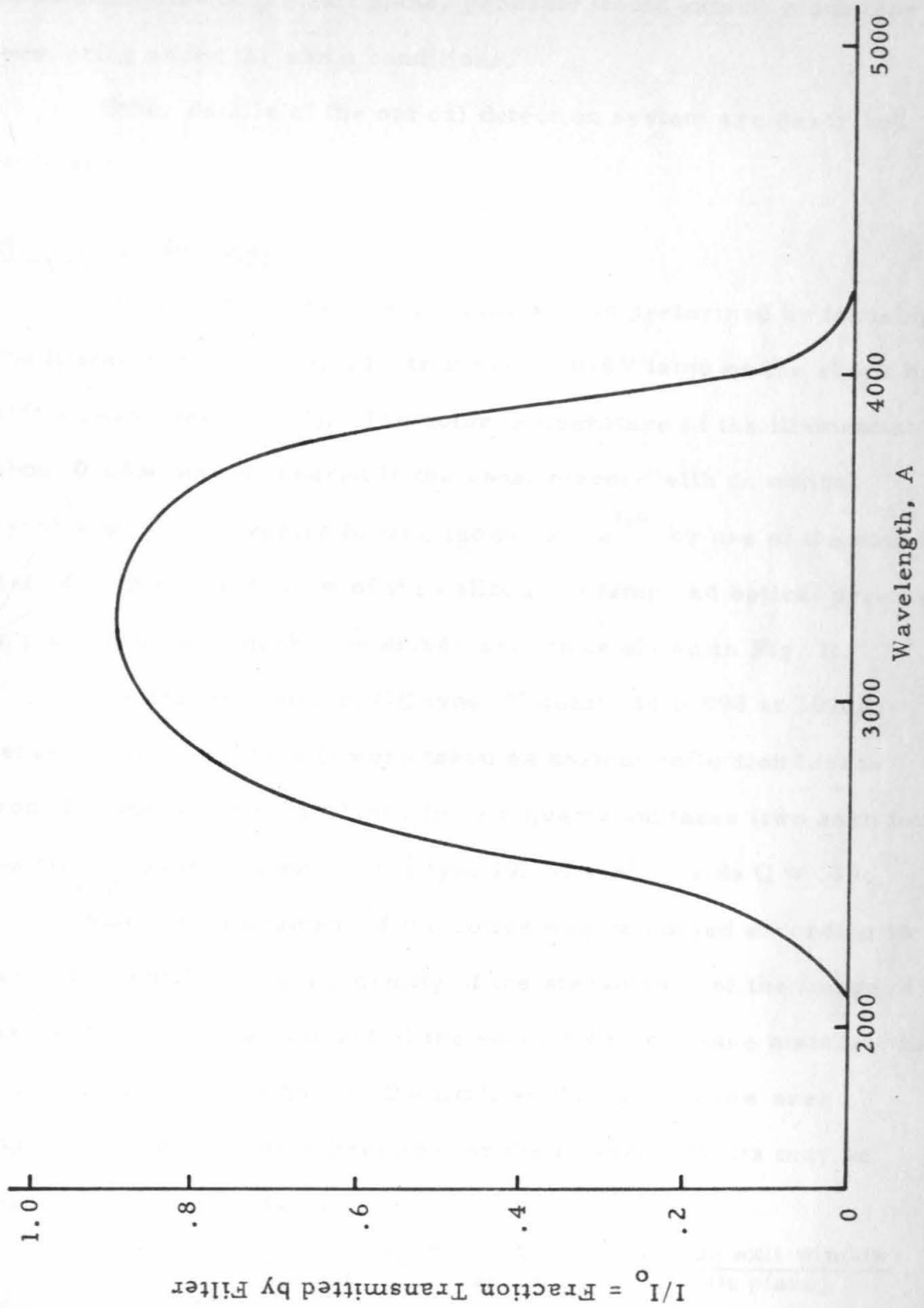


Fig. 10. Transmission spectrum of the Corning 7-54 filter.

photomultiplier in the exit plane, probably would exhibit much less scattering under the same conditions.

Other details of the optical detection system are described in Part I.

B. Calibration Optics

The absolute intensity calibration was performed by focusing the filament of a General Electric 30A/T24/6V lamp on the shock tube exit window (see Fig. 4). The color temperature of the filament at about 0.65μ was measured in the usual manner with an optical pyrometer and converted to true temperature⁽¹⁵⁾ by use of the data in Ref. 22. An overall view of the calibration lamp and optical pyrometer in place near the shock tube driver section is shown in Fig. 11.

The transmission of GE type 101 quartz is 0.998 at 3090A; hence the quartz losses Q were taken as normal reflection losses from Fresnel's formula which, for six quartz surfaces (two each for the lamp window and both of the type 101 lenses), yields $Q \approx .79$.

Since the placement of the optics was computed according to paraxial formulas, the uniformity of the steradiancy of the image of the calibration lamp filament at the shock tube end plane matches that of the actual filament only in the limit as the exit window area approaches zero. The correction for the off-axis effects may be approximated by the factor

$$= \frac{\text{calibration voltage/unit area of shock tube exit window}}{\lim_{A \rightarrow 0} (\text{calibration voltage/unit area at exit plane})} .$$

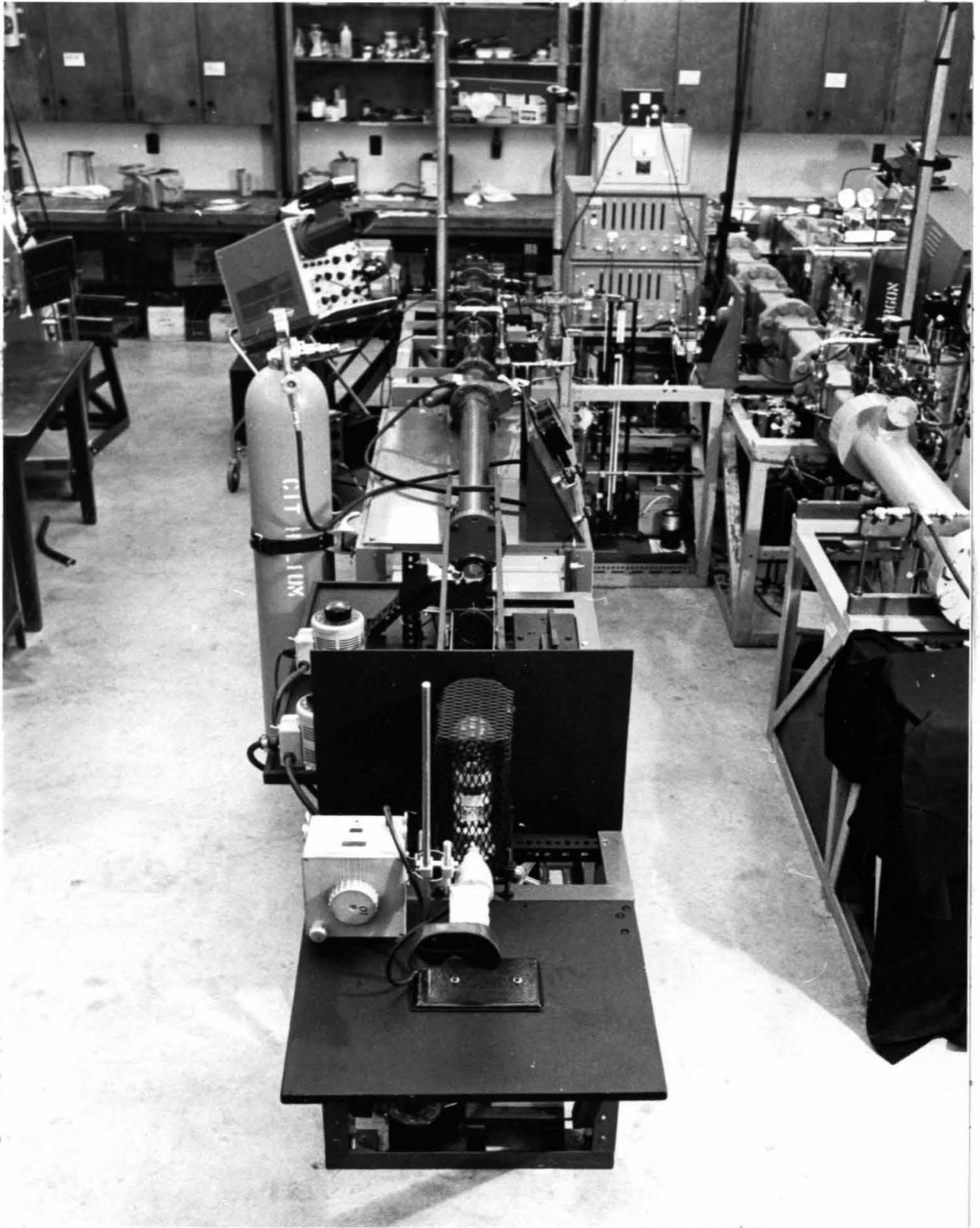


Fig. 11. A view of the calibration lamp and optical pyrometer in place at the driver end of the shock tube.

By using a set of different apertures at the exit window location, β was determined to be about 0.80 within $\pm 10\%$. The requirement that the calibration lamp output fill the angle 2α was checked by verifying that the calibration signal per unit aperture area A_L in Fig. 1 was linear up to the maximum value used for the experiments.

The linearity of response of the photomultiplier output was checked at signal strengths corresponding to those from the shock tube experiments by using the calibration lamp output in the visible region.

An absolute intensity calibration was performed immediately after each shock tube experiment to insure that all gain settings, optical alignments, etc., were constant.

IV. THERMODYNAMIC PROPERTIES OF THE GAS BEHIND THE SHOCK WAVE

As described in Part I, conditions behind the reflected shock were taken from IBM 7090 machine computations performed at the Aerospace Corporation in Los Angeles. National Bureau of Standards thermochemical data⁽²⁵⁾ were used, except that the heat of formation at 0°K for OH was taken as +9.27 kcal/mole.⁽²⁶⁾ Plots of the temperature and OH concentration in the reflected shock region, and the reflected shock velocity, u_{sr} , as functions of incident shock velocity are shown in Figs. 12-14. Note that these figures contain corrections of the data reported in Ref. 1.

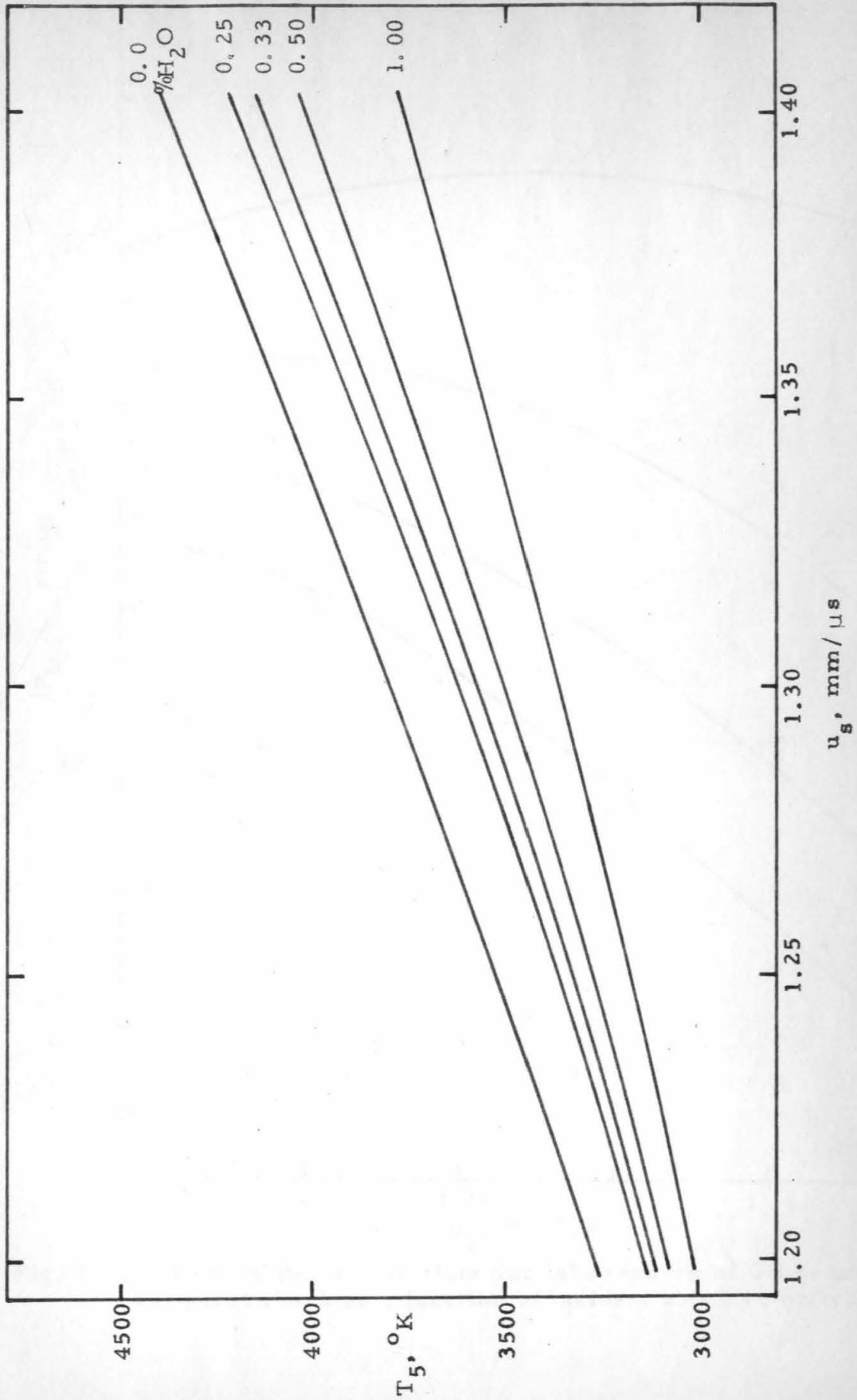


Fig. 12. The calculated equilibrium temperature T_5 behind the reflected shock as a function of incident shock velocity.

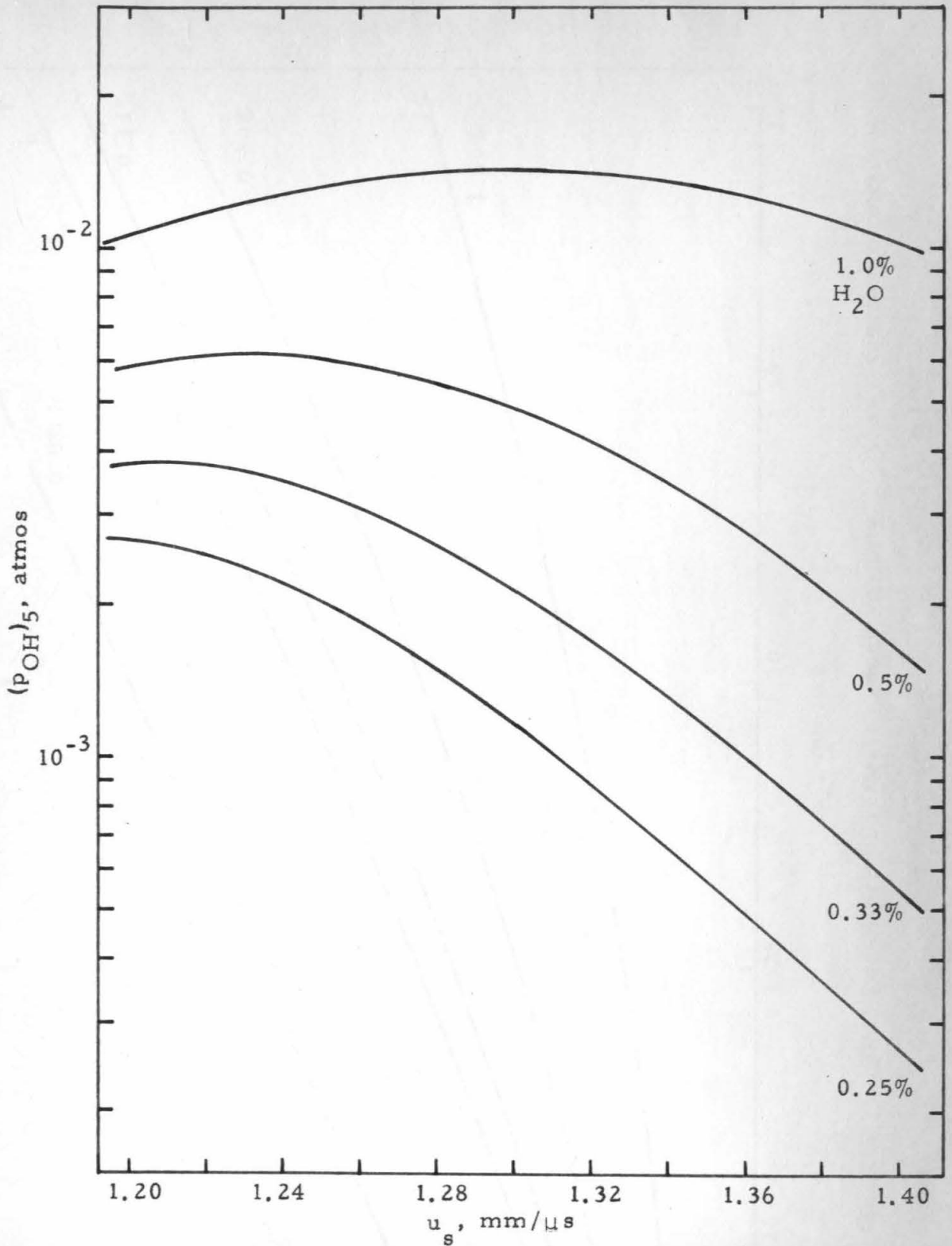


Fig. 13. The calculated equilibrium partial pressure of OH behind the reflected shock as a function of incident shock velocity.

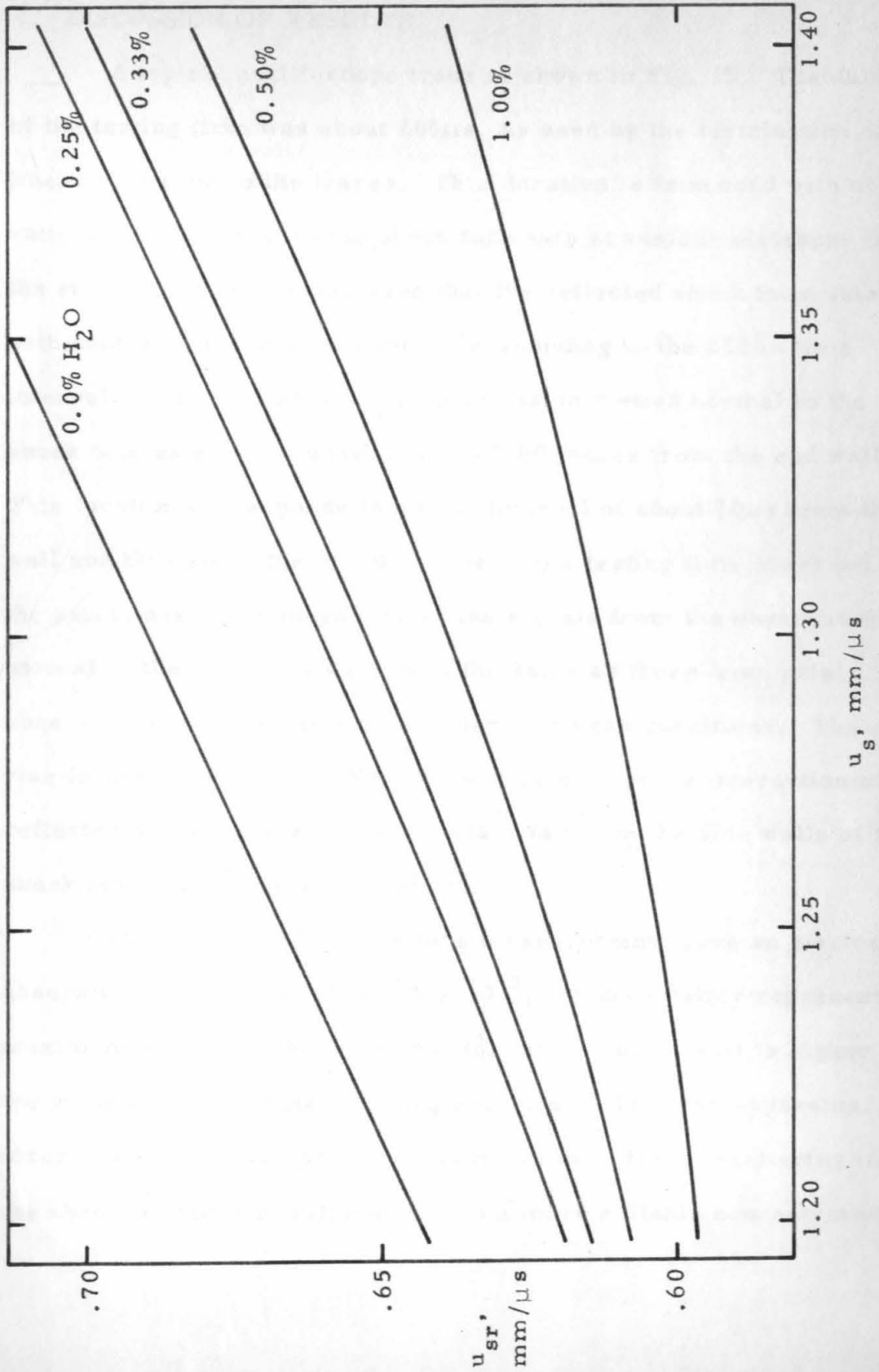


Fig. 14. The calculated equilibrium reflected shock velocity, u_{sr} , as a function of incident shock velocity.

V. DISCUSSION OF RESULTS

A typical oscilloscope trace is shown in Fig. 15. The duration of the testing time was about $200\mu\text{s}$, as seen by the termination of the linear rise time in the traces. This duration is in accord with observations made normal to the shock tube axis at various distances from the end wall, where it was seen that the reflected shock front interacted with another wave at a location corresponding to the $200\mu\text{s}$ time interval. Figure 16 shows the OH emission viewed normal to the shock tube axis at a window location 1.80 inches from the end wall. This location corresponds to a time interval of about $70\mu\text{s}$ from the end wall and thus about the middle of the $200\mu\text{s}$ testing time observed in the axial runs. The magnitude of the signals from the observations normal to the tube-axis was about the same as those from axial observations for the same optical depth and gas conditions. The slow rise in intensity shown in Fig. 16 is attributed to the interaction of the reflected shock wave with the boundary layer on the side walls of the shock tube, as discussed in Ref. 14.

The results of 15 shock tube measurements gave an electronic absorption f-number of $(3.9 \pm 0.9) 10^{-3}$, the uncertainty representing the maximum scatter in the experimental data. This result is higher than the value reported in Ref. 1 using essentially the same apparatus, the discrepancy being due primarily to the elimination of scattering in the absolute intensity calibration and a more reliable concentration

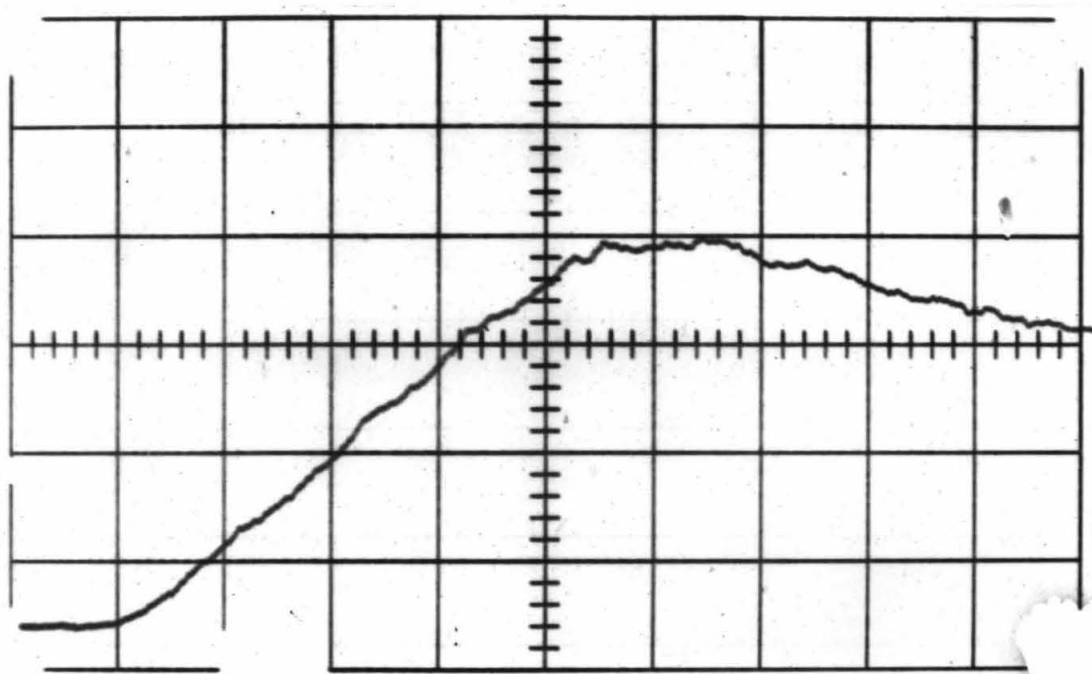


Fig. 15. A typical oscilloscope record for a shock tube test with observation of the emission in the axial direction behind the reflected shock wave. Sweep speed = $50 \mu\text{s/cm}$; gain = 10mv/cm ; initial H_2O concentration = 0.30% .

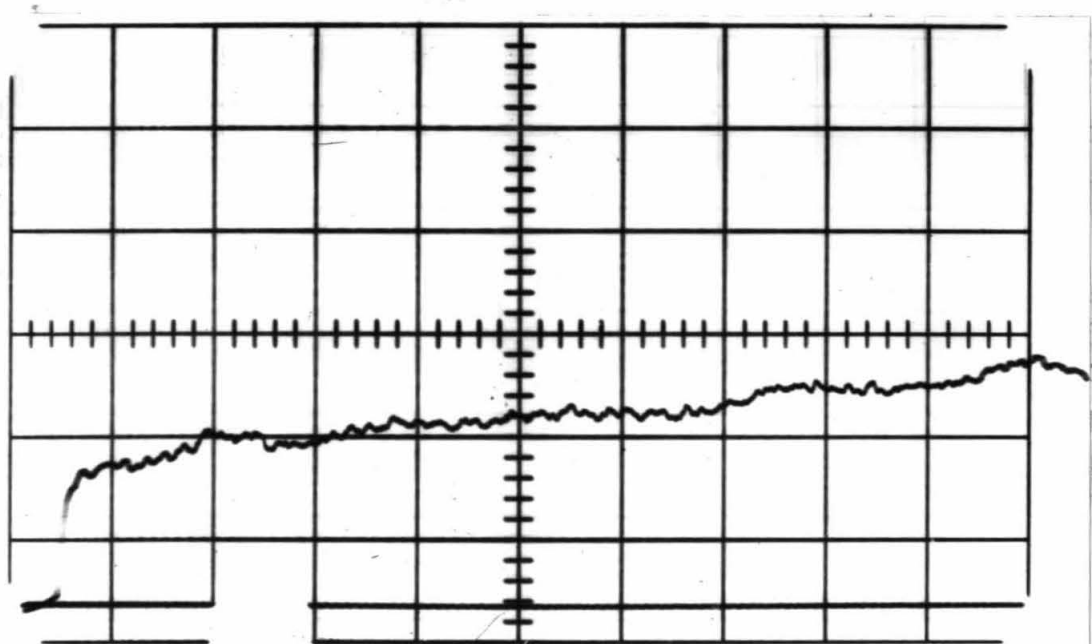


Fig. 16. Oscilloscope record of the OH emission behind the reflected shock wave viewed normal to the shock tube axis at 1.80 inches from the end wall. Sweep speed = $200 \mu\text{s/cm}$; gain = 50mv/cm ; initial H_2O concentration = 0.50% .

preparation for the present measurements. Approximate corrections applied to the data of Ref. 1 lead to good agreement with the present set of measurements.

The light scattering checks outlined in the section on Experimental Equipment have shown that errors in the f-number from this source are less than $\pm 5\%$. Impurity radiation levels contributed less than $1/2\%$ of the signals from the f-number experiments as determined from measurements of shock tube runs using pure argon test gas introduced into the tube with the usual flushing procedure but without using the water flasks in the mixing system.

The shock tube f-number is larger than that derived from furnace and flame measurements. However, the reliability of our data has been established since adequate care has been exercised in eliminating large errors from light scattering, impurity radiation, and uncertainties in test gas concentration. Furthermore, the technique of observing radiation axially behind the reflected shock wave, in a narrow core of hot gas, showed that the OH was transparent and that chemiluminescence was not present since the initial intensity rise shown in Fig. 15 is linear.

A possible source of systematic error in the shock tube experiments, which would result in a high f-number, is the existence of an overshoot in the population of OH behind the reflected shock wave

above that determined from the equilibrium calculations on which the f-number is based. The spectroscopic temperature measurements of Part I have established that internal statistical equilibrium has been reached for the vibration-rotation energies of the OH at the calculated equilibrium temperature. The likelihood that chemical equilibrium is not reached seems remote because of the long period of relatively steady radiation observed normal to the tube-axis, as shown in Fig. 16. During the $200\mu\text{s}$ testing time of the linear intensity rise in the axial observations, the OH molecules undergo about 10^6 collisions.

REFERENCES FOR PART II

1. M. Lapp, J. Quant. Spectr. Radiat. Transfer 1, 30 (1961).
2. T. Carrington, J. Chem. Phys. 31, 1243 (1959).
3. O. Oldenberg and F.F. Rieke, J. Chem. Phys. 6, 439 (1938).
4. P.J. Dyne, J. Chem. Phys. 28, 999 (1958); Guggenheim Jet Propulsion Center TR No. 12, Contract Nonr-220(03), NR 015 210, California Institute of Technology, November 1953.
5. R.W. Ditchburn, (Sec's 15.18-15.24), Light, Interscience Publishers, Inc., New York, 1953.
6. S.S. Penner and R.W. Patch, Radiative Transfer Studies and Opacity Calculations for Heated Gases, Guggenheim Jet Propulsion Center TR No. 6, Contract AF 49(638)-984, California Institute of Technology, January 1962.
7. L.H. Allen, Astrophysics: The Atmospheres of the Sun and Stars, Ronald Press Co., New York, 1953.
8. R. Watson, Spectroscopic Temperature Measurements on the $\text{OH}^2 \sum \rightarrow ^2 \Pi$ Band System for a Transparent Gas in a Shock Tube, Guggenheim Jet Propulsion Center TR No. 39, Contract Nonr-220(45), NR 015 401, California Institute of Technology, June 1962.
9. T.M. Helliwell, Ap. J. 133, 566 (1961); G.D. Bell and R.B. King, Ap. J. 133, 718 (1961).
10. R.G. Bennett and F.W. Dalby, J. Chem. Phys. 31, 434 (1959).
11. R.G. Bennett and F.W. Dalby, J. Chem. Phys. 32, 1716 (1960).
12. C.E. Treanor and W.H. Wurster, J. Chem. Phys. 32, 758 (1960).
13. R.A. Allen, J.C. Camm and J.C. Keck, J. Quant. Spectr. Radiat. Transfer 1, 269 (1961).
14. W.H. Wurster, J. Chem. Phys. 36, 2111 (1962).

15. S. S. Penner, Quantitative Molecular Spectroscopy and Gas Emissivities, Addison-Wesley Publishing Co., Reading, Mass., 1959.
16. L.H. Allen, Ap. J. 97, 135 (1943); L. Huldt and A. Lagerquist, J.O.S.A. 42, 142 (1952).
17. T.D. Wilkerson, The Use of the Shock Tube as a Spectroscopic Source with an Application to the Measurement of gf-Values for Lines of Neutral and Singly Ionized Chromium, Ph. D. Thesis and University of Michigan Department of Physics Report No. 02822-3-T, June 1961.
18. J.C. Keck, J.C. Camm, B. Kivel and T. Wentink, Jr., Ann. Phys. 7, 1 (1959).
19. S.S. Penner, J. Chem. Phys. 20, 507 (1952); 21, 31 (1953).
20. G.H. Dieke and H.M. Crosswhite, J. Quant. Spectr. Radiat. Transfer 2, 97 (1962).
21. R.W. Nicholls, Proc. Phys. Soc., A, Vol. LXIX, 941 (1956).
22. Tables for the Spectral Radiant Intensity of a Blackbody and of a Tungsten Ribbon, Research Report No. 59-32, Rocketdyne Division of North American Aviation, Inc., Canoga Park, Calif., 1959.
23. S.S. Penner, Chap. XVI, Chemistry Problems in Jet Propulsion, Pergamon Press, New York, 1957.
24. R. Watson, Rev. Sci. Instr. 10, 1113 (1962).
25. NBS Circular 500, Selected Values of Chemical Thermodynamic Properties, Washington, D. C., February 1952.
26. R.F. Barrow, Arkiv Fysik 11, 281 (1956). Also private communication with H. W. Wooley, National Bureau of Standards.